*Highlights

Behaviour of rehabilitated RC beams with self-compacting concrete jacketing – Analytical model and test results

- Thin reinforced self-compacting concrete jackets used to rehabilitate concrete beams
- Examined jackets combine high performance efficiency with known retrofit advantages
- Full recovery and favourable failure modes of the retrofitted beams are reported
- Analytical model to evaluate full response of the jacketed member is developed
- Tests correlated through member analysis considering interfacial force transfer

Behaviour of rehabilitated RC beams with self-compacting concrete jacketing – Analytical model and test results

Constantin E. Chalioris*[1], Civil Engineer, MSc, PhD, Assistant Professor

Georgia E. Thermou[2], Civil Engineer, MSc, PhD, Lecturer

Stavroula J. Pantazopoulou[3], Civil Engineer, MSc, PhD, Professor

[1] *Civil Engineering Dept., Democritus University of Thrace, Xanthi 67100, GREECE*

[2] *Civil Engineering Dept., Aristotle University of Thessaloniki, Thessaloniki 54124, GREECE*

[3] *Civil and Environmental Engineering Dept., University of Cyprus, Nicosia 1678, CYPRUS*

* corresponding author: tel./fax: +30 25410 79632 – email: chaliori@civil.duth.gr

Abstract

The use of thin reinforced self-compacting concrete jackets as a method to repair and strengthen under-designed flexural concrete members is investigated by means of experimental and analytical studies. The experimental component comprises 20 beam tests that were designed to fail mostly in shear either prior to, or immediately after flexural yielding with no ductility. After initial loading to near failure, specimens were repaired with three-sided jackets having the minimum thickness required in order to provide adequate bar cover and were subsequently retested to demonstrate the strength and ductility enhancement that could be attained through the intervention. The experimental results are correlated through member analysis considering the interfacial force transfer and relative slip occurring along the contact surface between new and existing concrete. The efficacy of the repair procedure and

the important parameters controlling the post-repair response are highlighted through consistent evaluation of the confining action exerted by the jacket on the encased core using equilibrium of forces and a frictional model. It is shown that with proper anchorage, the repaired members approach the strength, ductility, deformation capacity and model of failure of the ideal monolithic member having identical reinforcement details.

Keywords: Reinforced Concrete Beams; Self-Compacting Concrete Jackets; Repair; Retrofit; Flexural Strengthening; Upgrading of Shear Strength; Interface; Shear Transfer; Friction; Slip

1. Introduction

Thin Reinforced Concrete (RC) layers used as jacketing is a relatively recent development in the field of repair and rehabilitation of RC members [1-11] that became possible with the development of high strength Self-Compacting Concrete (SCC). The procedure combines the advantages of conventional RC jackets [12-17], namely stiffness increase, protection and development of the embedded longitudinal and transverse steel reinforcement of the jacket, with those provided by FRP jackets [17-29], such as the negligible alteration of member dimensions. Although FRP jackets are still much thinner than any thin RC jacket, considering the overall sectional dimensions, the differences between these two jacketing techniques appear small when compared to the solution of the conventional thick RC jacket that significantly increases the member size, changes stiffness and alters the dynamic characteristics of the building [1, 30, 31].

Several variations of the basic scenario have already been reported in the literature [32-34]. In all cases the jacket comprises a remarkably thin layer of fine-aggregate concrete, not exceeding 25 mm in thickness. The jacket is attached on the external faces of an existing RC member and encases a grid of small-diameter longitudinal and transverse steel bars. To facilitate casting, self-compacting concrete mixes are used as a matrix of the reinforcement in this application. This departs from the conventional methods of RC jacketing where concrete is placed through shotcreting that leads to layers at least 50-70 mm thick, effecting a significant alteration to the geometrical proportions of the jacketed member. In all jacketing methods an issue of critical importance is the degree of adhesion and interaction between the existing member (which functions as the core in the repaired condition) and the outer shell provided by the jacket [35-37]. This relies on the mobilisation of frictional mechanisms between old and new concrete, enhanced by the use of dowels [38].

In retrofitting procedures with any type of jacketing the strength enhancement is gauged by (a) the alteration of the mode of prevailing failure imparted by the jacket, and (b) the monolithic-effectiveness coefficient of the retrofit, which are obtained from the ratio between the strength of the jacketed member as compared with the corresponding values of monolithic members with identical geometry.

Most of the available experimental investigations, whether they concern shotcreted (thick) jackets or ultra-thin shells, were conducted on members with a rectangular cross section jacketed on all sides. According to previous investigations, full jacketing mobilizes confining pressures by the perimeter stirrups of the jacketing shell, which effectively increase the frictional strength and resistance against relative slippage at the interface between the core and the outer shell [35-41]. This favourable arrangement is not always possible in practical applications, either when applied to edge columns at the property line of structures in contact with adjacent buildings, or in the case of beams monolithically connected with floor slabs where only three-sided jacketing is possible. This paradigm motivated the study in the present investigation.

The experimental program comprises 20 RC beams representative of older detailing practices where inadequate stirrup spacing led to premature shear failure (prior to yielding of longitudinal reinforcement). Tests were conducted under four-point static loading (monotonic or cyclic). Three sided jacketing was applied as a means of repair and retrofit prior to reloading the specimens to failure, using the same loading setup as in the original loading phase. The potential of this new composite jacketing as a strengthening/repair procedure was illustrated from the experimental evidence.

Behaviour of most of the retrofitted specimens was modified substantially by altering the shear modes of failure observed in the initial damage state in flexural modes of failure. Only one specimen with significant longitudinal steel reinforcement and, thus, significant

shear demand exhibited also shear response after the addition of the jacket, since the span-to-depth ratio was less than 2 and, therefore, even after retrofitting the beam was predisposed to shear failure. Failure in most cases occurred by slippage at the interface between the existing (core) beam member and the jacket shell after the development of relative drift ratios in the range of 15%. In most of the specimens considered this occurred however after a substantial enhancement of flexural and shear strength of the specimens, accompanied by a substantially extended plastic response curve.

To facilitate interpretation of the experimental results, the response curve of the retrofitted test specimens was estimated using the dual section analysis procedures for RC jacketed members proposed by Thermou et al. [42]. In this analytical method, the magnitude of shear flow sustained along the contact surface is calculated by considering the states of stress of the composite member at a cracked cross section and at a point between successive cracks, in order to introduce in the flexural behaviour the effect of the moment gradient (shear force magnitude).

The following sections of the paper summarize the experimental and analytical components of the investigation and provide the values of monolithic effectiveness as a performance index of the proposed retrofit method. Objective of the paper is to demonstrate and fully document through experimental and analytical evidence the applicability and effectiveness of thin reinforced SCC jacketing as a retrofitting scheme for lightly-reinforced concrete members with details representative of older construction.

2. Experimental evaluation of thin RC jackets

In retrofitting damaged reinforced concrete members with reinforced SCC jackets an objective is to recover the original strength and to enhance the overall performance, without causing a significant alteration in the dimensions of the retrofitted component. Here, a dense

network of fine reinforcement in a very thin shell of self-compacting concrete is the basic ingredient of the retrofit methodology. Jacket reinforcement is placed practically on the surface of the existing element, with dowels used to enhance connectivity and force transfer at the interface between old and new concrete. Therefore, jacket thickness serves mostly for cover of the added reinforcement. Behaviour at the interface controls strengthening efficiency, particularly with regards to slip and deformation capacity (in terms of mid-span beam deflection and cracking patterns).

To interpret the role of the interface in the response, a dual-section analysis model is adapted to the requirements of reinforced SCC jacketed flexural elements. The study is based on an extensive experimental investigation involving twenty tests on flexural reinforced concrete beams. Specimens were retrofitted and retested after they had been originally damaged to failure under quasi-static load.

2.1. Characteristics of the tested beams

Beam specimens in this study are classified in two groups (A & B) based on their cross-sectional dimensions. Initially, group A specimens (A1 & A2) had width b_o = 200 mm, height h_o = 300 mm and effective depth d_o = 275 mm. The reinforcement of beam A1 consisted of longitudinal deformed steel bars with 14 mm diameter bars (2∅14 bars at the top and 2∅14 bars at the bottom of the cross-section of the beam) and deformed steel 8 mm diameter closed stirrups distributed at a uniform spacing of 200 mm. Beam A2 had 3∅16 bars at the top and 3∅16 bars at the bottom of the cross-section and contained no transverse reinforcement.

The cross-sectional dimensions of the initially tested specimens of group B were, b_o = 125 mm, h_o = 200 mm and d_o = 175 mm. Longitudinal reinforcement comprised of deformed steel 8mm diameter bars (2 or 4 ∅8 compression bars at the top and 2 or 4 ∅8

tension bars at the bottom of the beams' cross-section) and 5 mm diameter mild steel closed stirrups distributed at a uniform spacing of 300, 200 and 150 mm.

The measured tensile yield strengths of the ∅8 deformed steel reinforcement and the ∅5 mild steel stirrups were 570 MPa and 255 MPa, respectively. Further, the yield strengths of the ∅16 and the ∅14 deformed steel bars were 560 MPa and 590 MPa, respectively. Reinforcement arrangements, geometrical and mechanical characteristics of the initially tested beams are shown schematically in Figure 1 and summarized in Table 1. The concrete mean compressive and tensile strength ($f_{c,o}$ and $f_{ct,o}$, respectively) of each original beam were measured from compression and splitting tests of six cylinders per testing, respectively, and presented in Table 1 (subscript *o* refers to the properties of the original beam which serves as core of the jacketed member; subscript *J*, where it appears, refers to properties of the jacketed members).

The beam specimens had undergone severe cracking and substantial damage when loaded to failure in the initial test phase. All damaged specimens were repaired in the unloaded state, after removal of concrete fragments and straightening of the beams with marginal pressure. Specimens were rehabilitated using 25 mm thick reinforced SCC jackets that encased the bottom width and both vertical sides of the beams (U-shaped jacketing). This way, the retrofitted beams of group A had rectangular cross-sectional total dimensions equal to b_J/h_J = 250/325 mm and an effective depth d_J = 305 mm (i.e., t_J = 25 mm). Similarly, the cross-sectional dimensions of jacketed beams of group B were b_J/h_J = 175/225 mm and d_J = 205 mm. The total span of the jacketed beams remained the same as that of the initially tested beams, as shown in Figure 1(a).

The steel reinforcement of the jacket consisted of small diameter ∅5 mild steel with average yield strength equal to 255 MPa. Straight bars and U-formed stirrups were provided as longitudinal and transverse reinforcement of the jacket, respectively. Jacketing

reinforcement of the retrofitted specimens is displayed in Figure 1 and summarized in Table 1. Note that the total reinforcement ratios of the jacketed beams listed in Table 1 have been calculated based on the sum of the tension bars and the stirrups of each original beam and the respective reinforcements of the jacket.

2.2. Rehabilitation procedure

Jacketing was intended to increase the amount of the available reinforcement in order to increase flexural or/and shear resistance of the damaged specimens so as to fully recover their strength and to alter the pattern of failure to a more ductile mode.

Since the beams had sustained extensive diagonal or/and flexural cracking in the initial loading phase along with spalling of concrete cover, repair involved extensive intervention: all loose concrete fragments were completely removed and the missing parts of the beams were reconstructed followed by jacketing using form-casted SCC. No special roughening of the surface of the damaged beams was performed prior to jacketing. L-shaped 5 mm diameter mild steel dowels were installed on the vertical sides of the damaged beams in order to support the longitudinal bars of the jacket.

Dowels were bonded by injected epoxy resin into drilled 7 mm diameter holes. The number of dowels was rather low whereas no dowels were installed at the bottom face of the specimens to avoid further deterioration of the already damaged cover. These dowels were anchored through hooks that extend approximately 50 mm into the body of the composite beam (about 50 mm into the old concrete). Every side longitudinal bar of the jacket had ∅5 dowels per approximately 300 and 200 mm in jacketed beams of A and B series, respectively. Details of the installed dowels of each specimen are also presented in Figure 1(b).

Cast-in-place SCC was used to complete the rehabilitation procedure of the damaged beams. Mix proportions per cubic meter of the SCC used in the jackets are summarized in the

endnote of Table 1. Mean values of the cylinder compressive strength, $f_{c,J}$, and splitting tensile strength, $f_{ct,J}$, of SCC used for each jacketing application are also given in Table 1 (mean values of six cylinders for each batch).

2.3. Test setup and loading

During testing under four-point loading shear span was 800 mm for the beams A1 and A1-J and 600 mm for all the other specimens (see also Fig. 1(a)). Table 1 lists the span-to-depth ratios along with the geometric and reinforcing details of all specimens tested (original and jacketed beams). Note that after jacketing, through control of the amount of added reinforcement, beams with different initial number of bars attained comparable amounts of tension reinforcement (e.g. B3-J, B4-J and B5-J). Applied load and corresponding deflections were continuously monitored throughout the tests. Deflections of the tested beams were recorded by three LVDTs at mid-span and roller supports, located as shown in Figure 1(a). The difference between the LVDTs at the centre and the end supports is the relative displacement at mid-span occurring solely due to beam deformation (thus, spurious effects owing to the possible movement of the supports were filtered out from the mid-span deflection record).

The original beams B3R, B4R & B5R and the corresponding jacketed beams B3R-J, B4R-J & B5R-J were tested under repeated loading (identified by letter R in the specimen code name) using three and five cycles of loading-unloading-reloading per displacement level, respectively. All other specimens were tested monotonically to failure. Where applied, the objective of the cyclic loading sequence was to obtain data regarding the influence of load cycles and possible interfacial degradation at the jacket-core contact surface on the effectiveness of the applied reinforced SCC jacket.

Prior to the final loading step to failure, beams B3R, B4R & B5R were loaded and unloaded in two steps. In the first step, beams were subjected to monotonically increasing loads until visual detection of the first inclined cracking (onset of shear cracking) - which corresponded to approximately 50% of the ultimate load- and were subsequently unloaded. Note that the ultimate applied load had already been determined from the monotonic tests of identical beams B3, B4 and B5, respectively. In the second step, beams were loaded until formation of a single severe diagonal crack, corresponding approximately to 85% of the ultimate load and were then unloaded. Finally, in the third loading step, beams were loaded to failure.

Jacketed beams B3R-J, B4R-J & B5R-J were loaded and unloaded in four steps prior to the final loading step to failure. The first two steps were in the elastic range (prior to yielding), whereas the third and fourth steps extended into the inelastic range (after yielding of tension reinforcement). In the first loading step in the elastic range, beams were loaded to approximately 50% of yield load and were subsequently unloaded (the yield load had been previously determined from monotonic loading of jacketed beams B3-J, B4-J & B5-J). In the second step (while specimens were still in the elastic range) beams were loaded to approximately 85% of yield load and subsequently unloaded. In the third step, beams were loaded beyond yielding to a displacement ductility of 1.5 and unloaded to zero load. In the fourth step (also in the inelastic range) beams were loaded to a displacement ductility of 8, and then unloaded, prior to being carried to failure in the fifth loading step.

2.4. Test results

Figure 2 plots the mid-span load versus deflection curves for each initially tested and subsequently jacketed beam pair. Values of measured load at the onset of flexural cracking, P_{flex}, at the onset of diagonal shear cracking, P_{diag}, at yielding, P_y, (if observed) and the

ultimate capacity, P_u, and the corresponding deflections (Δ_{Py} and Δ_{Pu}, respectively) of the initially tested and jacketed beams are also reported in Table 2. The observed strength and ductility enhancements obtained through jacketing were remarkable in most cases. Furthermore, performance of the jacketed beams was substantially improved in terms of the prevailing mode of failure: specimens B3-J, B3R-J, B4-J, B4R-J, B5-J and B5R-J exhibited a pure flexural mode whereas the initially tested beams B3, B3R, B4, B4R, B5 and B5R had experienced brittle shear failure. This improvement is quantified by the values of the displacement ductility capacity increase, Δ_{max}/Δ_{Py}, listed in Table 2. Cracking patterns at failure of the initially tested and the jacketed beams are highlighted in the photographs of Figure 3 and summarized in Table 2, respectively.

Comparisons between the monotonically tested beams and the corresponding specimens that were tested under repeated load cycles showed only a minor influence of cyclic loading on performance. Marginal reductions in the flexural strengths of jacketed specimens B3R-J, B4R-J & B5R-J (subjected to repeated loading) were observed with respect to the corresponding monotonically loaded jacketed specimens B3-J, B4-J & B5-J. This concurs with the marginal amount of hysteresis drawn by the load-displacement unloading-reloading cycles, suggesting that progression of damage was contained and response remained under control of flexural reinforcement yielding without any significant loss owing to cyclic degradation at the interfaces.

3. Analytical model

Full jacketing of RC members with rectangular cross section (four-sided jacket) mobilizes confining pressure by the perimeter stirrups of the jacket as shown in Figure 4a. This reinforcement in the present case of three-sided RC jacketed sections corresponds to the web reinforcement of the jacket (Fig. 4a). Any relative sliding between the two bodies in contact

(core and the jacket shell) causes transverse dilation due to the overriding of asperities of one surface over the other placing the reinforcement that crosses the contact plane into tension and gives rise to a passive clamping pressure σ_N acting normal to the contact surfaces. Pressure σ_N effectively increases the frictional resistance against relative slip between the existing member (core) and the jacketing shell (Fig. 4b).

In the examined case of a three-sided jacket (U-jacketing) it was found that the effect of interfacial slip on the response envelope of a jacketed beam member can be particularly significant on the deformation behaviour (Figs. 4b and c). Slip on the beam soffit between old concrete and the jacket serves to partially relieve stress in the tension zone while effectively increasing the amount of curvature and concrete compression strains to levels that would, in a monolithic situation, correspond to higher steel stresses and internal forces (Fig. 5b). For this reason, the constitutive behaviour of the contact surface is key ingredient for a complete analytical model of the jacketed member's behaviour: An overly strong interface would act as a monolithic contact and thus, slip would be suppressed. An overly compliant interface would lead to excessive drifts/deflections while composite member resistance would be significantly compromised.

To establish the state of stress in the jacket, longitudinal and transverse reinforcement is considered smeared (i.e., uniformly distributed) in the jacket cross-sectional area, having area ratios of ρ_l and ρ_t, in the longitudinal and transverse directions, respectively (Figs. 4c and d). This assumption is possible considering the density of the reinforcement arrangement achieved through the use of small diameter bars in most of the specimens (excluding B1-J and B2-J); a criterion is that a crack inclined at 45^o with respect to the longitudinal axis of the member intersects at least two different layers of reinforcement engaged in tension in each direction. An alternative criterion is that the regions of concrete not effectively engaged in tension stiffening in the tension zone should be minimal.

Furthermore, considering the small thickness of the jacket layer as compared to the other dimensions of the arrangement, the jacket layer is assumed to act primarily in plane stress (forces acting in the plane of the jacket layer.) Neglecting the tensile strength of concrete, the resultant membrane stresses that may be transferred through interfacial shear/bond from the jacket to the encased core over a distance equal to half crack spacing are defined as: $\sigma_t = \rho_t f_{s,t}$ and $\sigma_l = \rho_l f_{s,l}$, respectively (Fig. 4c, d for transverse reinforcement and Fig. 4e for longitudinal reinforcement of the jacket).

The stress resultant of the jacket membrane forces on a member cross section in the longitudinal axis of the member (local *l* and global x-axis), gives rise to an axial compressive load in the core cross section to maintain equilibrium (Fig. 4e). Through this action, stresses σ_l contribute directly to the flexural behaviour of the retrofitted member, whereas stresses σ_t (Fig. 4d) participate in the response mechanisms that are prerequisite to support the flexural response, namely (a) member shear strength through the added web reinforcement, (b) frictional interaction and cooperation between the outer shell and the core through actions at the contact surfaces (interfaces) of the two components. Contact forces depend on two sources of resistance: (b.1) the dowel action provided by mechanical anchors that are intended to prevent / resist relative slippage between the two components, v_{dowel}, and (b.2) the contact friction, $v_{friction}$, that is mobilized along the interfaces of the two components (i.e core and jacketing outer shell), the magnitude of which depends on the surface roughness and the clamping pressure, σ_N, acting normal to the interface (Fig. 4b). The latter components interact with the presence of confining perimeter stirrups wrapping the core member. It was stated that the asperities of the contact surface determine the maximum degree of dilation required by the jacket before sliding may be said to occur freely between the inner and the outer components (Fig. 4b, 4c), stretching the stirrups in tension and thereby mobilizing the passive confining

pressures σ_N. The frictional resistance of the interface is obtained according with a Mohr-Coulomb type of model as follows:

$$v_{int} = v_{dowel} + v_{friction} \quad (1)$$

$$v_{friction} = v_{adh} + \mu \cdot \sigma_N \quad (2)$$

In eq. (2) μ is the coefficient of friction, v_{adh} is the adhesion term of resistance against slippage of the contact surfaces. This term is neglected in the following calculations because it represents a weak source of strength that is easily compromised by hydration shrinkage of the jacket after casting.

To calculate the interface clamping pressure, σ_N (acting on the existing beam soffit), the uniformly distributed web reinforcement having an area ratio ρ_t in the jacket thickness is considered: $\sigma_N=2\sigma_t.t_J/b_o$ where t_J the jacket layer thickness, b_o the width of the original cross-section, and $\sigma_t=\rho_t f_{s,t}$ the jacket stress in the y-direction and $f_{s,t}$ the axial stress of the web reinforcement (Fig. 4c). In three-sided jacketing the normal pressure (σ_N) attains its peak value near the lower end of the cross section where stirrup stresses, ($f_{s,t}$) can depend on the longest possible development length (Fig. 4c). Unless the jacket is clamped near the ends of the three-sided arrangement, the transverse stress σ_t and the resulting interface pressure will inevitably attenuate towards the top end of the jacket following the pattern shown in Fig. 4c. Thus, along an inclined failure plane extending up to the neutral axis of the composite jacketed cross-section, contribution of the jacket to shear strength of the member is equal to (Fig. 4d):

$$V_J = 2t_J \int_{c_J}^{d_J} \sigma_t(z)dz = 2ave(\sigma_t) \cdot t_J \cdot (d_J - c_J) \quad (3a)$$

where c_J and d_J the depth of compression zone and the effective depth of the jacketed section, respectively, $ave(\sigma_t)$ is the average value of the transverse stress along y-axis in the tensile

zone (Fig. 4d) (see also Figs. 5a and b for notation). An average value of the pressure σ_N is obtained from equilibrium in the *t*-direction (*t* refers to the local axis in Fig. 4d, which coincides with the global axis y):

$$\sigma_N = 2ave(\sigma_t)\cdot t_J / b_o \tag{3b}$$

3.1. Interface shear behaviour

In the developed algorithm constitutive models are necessary in order to estimate the combined dowel and shear friction resistances for a given amount of slip (monotonic response). The methodology builds on formulations for jacketed columns by Thermou et al. [42] whereby contact friction and transverse cracking is modelled in order to account for slip as a degree of freedom between the internal core and the exterior jacket shell, occurring at the tension face of the encased beam. Necessary constitutive relationships are adapted from the recently launched Hellenic code for seismic retrofitting of existing structures [43]. A brief summary is presented here for the sake of completeness.

(a) Frictional resistance at interfaces: The lower contact surface between the interior core and the jacket shell is confined by normal pressure σ_N calculated from Eq. (3). The ultimate frictional resistance of the interface is defined with reference to σ_N according with:

$$v_{friction,u} = \mu\left(f_c^2 \sigma_N\right)^{1/3} \tag{4}$$

where μ = 0.4 is the ultimate interfacial shear-friction coefficient and f_c is the uniaxial compressive strength of the weakest concrete in the connection [43]; here this is taken to correspond, without loss of generality, to the strength of the encased core concrete of the original beam (i.e., $f_c = f_{c,o}$).

Term ρ_t corresponds to the web smeared reinforcement in the jacket thickness and $f_{s,t}$ is the stress in the web steel (stirrups) at the interface which, for uniform bond stresses along

the embedment length is equal to: $f_{s,t}=(0.3s^{2/3}E_s f_{c,o}/D_b)^{1/2}$ [44] where E_s is the elastic modulus of steel and D_b is the stirrup diameter of the jacket.

Shear stress at the interface is related to the relative slip between the contact surfaces (interface between the existing member and the jacket), s; a constitutive model describing the shear stress – slip relationship is given by the following equations [45]:

$$\frac{v_{friction}(s)}{v_{friction,u}} = 1.14\left(\frac{s}{s_{c,u}}\right)^{1/3} \text{ for } \frac{s}{s_{c,u}} \le 0.5 \quad (5a)$$

$$\frac{v_{friction}(s)}{v_{friction,u}} = 0.81+0.19\left(\frac{s}{s_{c,u}}\right) \text{for} \frac{s}{s_{c,u}} > 0.5 \quad (5b)$$

where, $s_{c,u}$ is the highest value of slip attained, beyond which the frictional mechanisms are assumed to break down (a value of 2 mm is recommended in [43] and [46]).

(b) Dowel resistance of the interface: The dowel model proposed by Vintzileou and Tassios [47, 48] is based on two assumptions: the steel bar behaves exactly like a horizontally loaded free-headed pile embedded in cohesive soil and that yielding of the dowel occurs simultaneously with crushing of the surrounding concrete. The relationship between developed dowel force and slip are described by:

$$\frac{V_{dowel}(s)}{V_{dowel,u}} = 0.5\frac{s}{s_{d,el}} \text{ for } s \le s_{d,el} = 0.006D_b \quad (6a)$$

$$\text{For } \frac{V_{dowel}(s)}{V_{dowel,u}} \ge 0.5 \Rightarrow s = 0.006D_b + 1.76s_{d,u}\left[\left(\frac{V_{dowel}(s)}{V_{dowel,u}}\right)^4 - 0.5\left(\frac{V_{dowel}(s)}{V_{dowel,u}}\right)^3\right] \quad (6b)$$

where $s_{d,el}$ is the elastic slip value, $s_{d,u}$ is the ultimate slip value, $V_{dowel,u}$ is the dowel strength and D_b is the diameter of the bars that provide dowel-type resistance (here, these are the stirrup legs of the jacket transverse reinforcement).

The dowel strength and associated interface slip are given by:

$$V_{dowel,u} = 1.3D_b^2\left(f_c f_{sy}(1-\beta)^2\right)^{1/2} \text{ and } s_{d,u} = 0.05D_b \quad (7)$$

where β is the bar axial stress normalized with respect to the corresponding yield strength, f_{sy} of the reinforcement.

3.2. Estimation of crack spacing and shear stress distribution

In the approach followed using the proposed analytical model for three-sided jacketed members, it is considered that in the initial stages of loading flexural cracks begin to form in the jacket upon exceedance of the tensile strength, $f_{ctm,J}$. The number of cracks increases gradually with increasing load, up to the onset of crack stabilization beyond which no new cracks are formed but rather the existing cracks start to widen and propagate gradually till failure. This occurs when the stress in the jacket longitudinal reinforcement at the crack, $f_{s,cr}$ exceeds the limit [46]:

$$f_{s,cr} > f_{ctm.J} \frac{1+\eta\rho_{l,tot}}{\rho_{l,tot}} \tag{8}$$

where $f_{ctm,J}$ is the tensile strength of the self-compacting concrete, $\eta(= E_s / E_{cm})$ is the ratio of the material moduli and $\rho_{l,tot}$ is the effective tensile reinforcement ratio defined as the total steel area divided by the area of mobilized concrete in tension [46]. After crack stabilization and as the load increases further, the cracks propagate and penetrate the core of the jacketed member (Fig. 5a). The crack patterns developed in the tested beams as presented in the photographs of Fig. 3 are in agreement with this assumption.

Similar to conventional bond analysis, shear transfer at the interface between the existing member and the jacket is carried out using dual section analysis between half crack intervals along the length of the jacketed member. To evaluate the crack spacing, the stress state at the crack is compared with that at the mid-span between adjacent cracks in the constant moment region where shear is zero (Fig. 5c). Assuming that the neutral axis depth, c_J, is about constant in adjacent cross sections after stabilization of cracking, the crack spacing, C_{cr}, is defined from the free body diagram of the composite section (see Fig. 5d

section A-A and section B-B). Thus, the shear stress at the interface between the jacket layer and the encased beam is estimated from two alternative approaches: (a) from the free body diagram of the jacket up to a height equal to the thickness of the jacket (Eqs. (9a)) and (b) from the free body diagram of the tension zone of the composite cross section down to the interface at the soffit of the encased beam (Eq. 9(b)) as:

$$N_J^{bot} f_{b,J} \cdot \pi D_{b,J} \cdot \frac{C_{cr}}{2} = \tau \cdot b_J \cdot \frac{C_{cr}}{2} + t_J \cdot b_J \cdot f_{ctm,J} \Rightarrow \tau = N_J^{bot} f_{b,J} \cdot \frac{\pi D_{b,J}}{b_J} - \frac{2 \cdot t_J \cdot b_J \cdot f_{ctm,J}}{b_J \cdot C_{cr}} \tag{9a}$$

$$\begin{aligned} & N_J^m \cdot f_{b,J} \cdot \pi D_{b,J} \cdot \frac{C_{cr}}{2} + N_o^{bot} f_{b,o} \cdot \pi D_{b,o} \cdot \frac{C_{cr}}{2} + \tau \cdot b_J \cdot \frac{C_{cr}}{2} = 2 t_J \cdot \ell_c \cdot f_{ctm,J} + b_o \cdot \ell_c \cdot f_{ctm,o} \\ & \Rightarrow \tau = 4 \cdot \frac{t_J}{b_J} \cdot \frac{\ell_c}{C_{cr}} \mathrm{f_{ctm,J}} + 2 \cdot \frac{b_o}{b_J} \cdot \frac{\ell_c}{C_{cr}} \mathrm{f_{ctm,o}} - N_J^m \cdot f_{b,J} \frac{\pi D_{b,J}}{b_J} - N_o^{bot} f_{b,o} \frac{\pi D_{b,o}}{b_J} \end{aligned} \tag{9b}$$

The crack spacing, C_{cr}, is estimated from the requirement that the shear stress value obtained from Eqs. (9a) and (9b) is the same:

$$\begin{aligned} & (N_J^{bot} + N_J^m) f_{b,J} \frac{\pi D_{b,J}}{b_J} + N_o^{bot} f_{b,o} \frac{\pi D_{b,o}}{b_J} = \frac{t_J}{b_J C_{cr}} \left[2 \cdot b_J + 4 \cdot \ell_c \right] f_{ctm,J} + 2 \cdot \frac{b_o}{b_J} \cdot \frac{\ell_c}{C_{cr}} f_{ctmo} \Rightarrow \\ & C_{cr} = \frac{t_J [2 b_J + 4 \ell_c] f_{ctm,J} + 2 b_o \ell_c f_{ctm,o}}{(N_J^{bot} + N_J^m) f_{b,J} \pi D_{b,J} + N_o^{bot} f_{b,o} \pi D_{b,o}} = 0.64 \frac{t_J \cdot [b_J + 2 \ell_c] f_{ctm,J} + b_o \ell_c f_{ctm,o}}{(N_J^{bot} + N_J^m) f_{b,J} D_{b,J} + N_o^{bot} f_{b,o} D_{b,o}} \end{aligned} \tag{9c}$$

where t_J is the thickness of the jacket, ℓ_c is the height of the tension zone in the core component of the composite cross section (Fig. 5d), $f_{ctm,o}$ and $f_{ctm,J}$ are the tensile strengths of concrete core and jacket, respectively, b_J and b_o are the widths of the jacket and core sections, respectively, N_o^{bot} is the number of bars in the tension steel layer of the core, N_J^{bot} and N_J^m are the number of bottom and side bars in the tension steel layer of the jacket, $D_{b,o}$ and $D_{b,J}$ are the bar diameters of the core and the jacket longitudinal reinforcement, respectively, $f_{b,o}$ and $f_{b,J}$ is the average bond stress of the core and jacket reinforcement layer, respectively (according to EC-2 [49] f_b is taken equal to $2.25 f_{ctm}$ for ribbed bars, and f_{ctm} for smooth bars).

In case of the beams studied herein, Eq. 9(c) may be simplified further by considering the average bond stress of the core equal to that of the jacket reinforcement layer taken equal to $f_{b,o} = f_{b,J} = 2.25 f_{ctm,o}$:

$$C_{cr} = \frac{1}{3.6} \cdot \frac{t_J \cdot (b_J + 2\ell_c) \cdot \lambda + b_o \ell_c}{(N_J^{bot} + N_J^m) D_{b,J} + N_o^{bot} D_{b,o}} \quad (9d)$$

where t_J is the thickness of the jacket, ℓ_c is the height of the tension zone in the core component of the composite cross section (Fig. 5d), b_J and b_o are the widths of the jacket and core sections, respectively, N_o^{bot} is the number of bars in the tension steel layer of the core, N_J^{bot} and N_J^m are the number of bottom and side bars in the tension steel layer of the jacket, $D_{b,o}$ and $D_{b,J}$ are the bar diameters of the core and the jacket longitudinal reinforcement, respectively, and $\lambda = f_{ctm,J} / f_{ctm,o}$. Eq. 9(d) was adopted for calculating the crack spacing values, C_{cr}, that appear in Fig. 3.

Shear stress demand at the interface, τ_d, is determined by examining the cross section along the height and along a member length equal to the distance between successive cracks (i.e., a dual section analysis is conducted as shown in Fig. 6). The normal force resultant ΣF (sum of forces in concrete and steel at height equal to the jacket thickness) is used to calculate the average shear stress demand in the web cross section of the member, τ_d. With the assumption that the shear flow, q, reverses sign approximately at $C_{cr}/2$ (where C_{cr} is the crack spacing), the average stress demand τ_d is equal to:

$$\tau_d = \frac{\Sigma F}{0.5\, C_{cr}\, b_J} \quad (10)$$

where, ΣF is the force resultant of the bottom layer equal to jacket thickness (i.e. the distance between the lower fiber of the composite cross section and the beam soffit interface), and b_J is the width of the jacketed cross section.

3.3. Calculation algorithm for moment versus curvature analysis

An algorithm was developed for flexural analysis allowing for slip between the contact interface of the core section and the jacket. A flowchart of the developed algorithm is shown in Fig. 7. The main objective is to satisfy the constitutive laws for the interface (i.e., shear

stress demand at the interface for a magnitude of relative slip, s, be equal to the shear stress capacity for that slip magnitude – which corresponds to the first set of loops in Fig. 7) while at the same time satisfying force equilibrium over the cross section (second set of loops in Fig. 7). The procedure followed is iterative till convergence is secured (i.e. the point when the error norm is reduced below a predefined tolerance specified by the user). At very low curvature values, φ, the composite cross section behaves monolithically, simulating successfully the resistance to sliding due to cohesion between the contact interfaces. With increasing curvature, the gradient of the strain profile is modified (allowing a gradual discontinuity of strain at the interfaces) in order to satisfy cross sectional equilibrium. Hence, for each loading cycle, the sectional curvature, φ, is established with reference to the profile of normal compressive strains of the composite cross section, (ε_{J1} is the axial strain at the top fibre and c_J the associated depth of compression zone) whereas the slip at the interface is obtained from the strain difference between core and jacket at that level (Fig. 5b):

$$\phi = \frac{\varepsilon_{J1}}{c_J} \text{ and } s = (\varepsilon_{J2} - \varepsilon_{J3}) \cdot \frac{C_{cr}}{2} \qquad \text{(11a \& b)}$$

The required steps in order to solve for the state of stress that satisfies the governing equilibrium and compatibility equations are as follows (see flowchart in Fig. 7):

- Step #1 – Assume a value for the sectional curvature φ^n.

- Step #2 - The normal strain at the top fiber of the cross section, $\varepsilon_{J1}^{n,m}$, is estimated.

- Step #3 - The slip at the interface, $s^{n,r}$, is estimated (Eq. (11b)).

- Step #4 - The associated shear capacity of the bottom interface, $\tau^{n,r}$, is estimated from the constitutive laws described in the preceding section. Shear demand, $\tau_d^{n,r}$, (Eq. (10)) is compared to shear capacity, $\tau^{n,r}(s)$. The slip, $s^{n,r}$, is modified further ($s^{n,r+1} = s^{n,r} + ds$; ds is the selected increment in the slip value) till attainment of equilibrium at the bottom interface (Fig. 7, first set of loops).

- Step #5 - If equilibrium at the bottom layer is satisfied, the next step involves attainment of equilibrium of the entire cross section at the location considered. If equilibrium is not satisfied, (i.e., if |ΣΣF over the entire cross section| > tolerance), then the normal strain profile is revised by setting a $\varepsilon_{J1}^{n,m+1} = \varepsilon_{J1}^{n,m} + d\varepsilon_{J1}$, where $d\varepsilon_{J1}$ is the step increment in the top strain of the jacketed cross section (Fig. 7, second set of loops).

- Step #6 - The convergent values for which equilibrium is satisfied at both the interface and at the cross sectional level are saved and the moment resultant, M^n, is estimated.

This procedure is repeated for each chosen curvature value. Seed values for the parameters at each new step are the last converged values of the previous steps. Calculations are terminated when the shear capacity of the interface is exhausted.

4. Comparisons between analytical predictions and test data

4.1. Analytical moment – curvature estimations

The analytical algorithm described in Section 3.3 was implemented for calculation of the moment – curvature envelopes of the three-sided jacketed beams. Obtained results are also compared with those derived from cross sectional analysis using Response 2000 [50, 51] for the sake of comparison (results of the latter approach are marked accordingly in the respective plots). A single value of concrete strength was used throughout the study in modelling the jacketed beams. For each case considered, the concrete strength was taken equal to the uniaxial strength of the initial (existing) member since the compression zone in the present problem occurs primarily in that component. The calculated moment versus curvature response curves of beams of group A and of representative beams of group B are shown in Figs. 8 and 9 along with the evolution of slip and interfacial average shear stress (at the encased beam soffit). Curves obtained by considering the slip at the interface between the existing cross section and the jacket are denoted as “Analytical”, whereas calculations that

neglect the slip effects are referred to as "Monolithic". The estimated crack spacing, C_{cr}, for which the analyses were obtained are marked on the specimen photos along with the corresponding experimental values, C_{cr}^{exp} (Fig. 3a and 3b). Curves denoted as "Monolithic" were obtained assuming perfect contact at the interface; results from the monolithic analysis are practically identical to those obtained from Response 2000. Furthermore, comparison between the analytical and monolithic response curves indicates that in all cases the two curves are very close, suggesting that the three-sided jacketed beams practically behaved almost monolithically until advanced stages of inelastic deformation.

The moment – shear failure envelopes at the instant of yielding of the bottom layer reinforcement of the jacket were derived with the use of Response 2000 [50, 51] and are plotted in Figs. 10 and 11. The failure envelopes provide a direct insight in the prioritizing of shear and flexural modes of failure for the retrofitted beams. In each graph of Figs. 10 and 11, the blue coloured curve corresponds to the calculated failure envelope, the vertical green dashed line depicts the flexural capacity at yielding for the case of monolithic response, whereas the vertical red coloured dashed line corresponds to the case when slip is taken into account (the proposed algorithm was used to model both the monolithic response and the response with slip). In the figure, the horizontal green and red dashed lines correspond to the estimated shear strength demand (SSD) at flexural yielding. SSD is the shear force in the beam when flexural yielding occurs in the constant moment region. It is obtained by dividing the yield moment of the beam cross section by the shear span, L_s . The shear span was equal to 0.8 m for beam A1-J and 0.6 m for all the other beams. The radial dashed line corresponds to the moment capacity - shear strength pair of values when flexure-shear interaction is accounted for, according with the modified compression field theory [51] (the slope is equal to the inverse of the shear span: V/M).

In order to interpret the estimated mode of failure is important to notice that in all failure envelopes there is negligible interaction between moment and shear in the lower right part of each graph where shear demand is very low. This is evidenced by the fact that moment strength remains unaltered for shear demand values that range between 0 (very long shear span) to about 1/5 of the nominal shear strength. For shear demands higher than that limit, flexural strength is compromised by the interaction with shear, the effect becoming more intense the higher the shear demand. In the latter case, shear failure is expected to occur if the performance point (with coordinates the analytic flexural strength and associated shear demand) falls either on, or outside the failure envelope (if the performance point is on the envelope, shear failure occurs immediately upon flexural yielding; if the performance point lies outside the failure envelope the shear failure is expected to follow at some point after flexural yielding). From the failure envelopes obtained, it is evident that only A2-J is anticipated to fail in shear simultaneously with flexural yielding. Specimen A1-J is expected to fail in shear after significant flexural yielding, whereas all the strengthened specimens in group B (where the performance point occurs inside the failure envelope) are controlled by flexural yielding.

4.2. Comparisons between analytical and experimental response curves

The derived moment – curvature response curves with the use of the proposed analytical model when slip at the interface is considered are transformed to load – mid-span deflection envelopes and are compared with the corresponding experimental curves in Figs. 12 and 13. In general, the analytical model curves are in good agreement the experimental ones. The sudden loss of strength in the case of specimen A1-J is attributed to fracture of the initial tension reinforcement (because part of the available strain capacity of that steel had been exhausted during the initial phase of testing, leaving a small residual strain range for the

response after strengthening). Specifically for the case of A2-J shear failure was anticipated based on the estimated failure envelope (discussed in the preceding section).

In the case of group B beams, as stated in section 4.1 the analytical deflection curves were practically identical to the monolithic ones. Comparison between the experimental load versus mid-span deflection curves with the corresponding analytical estimates shows some discrepancy in the post-yielding range of response (the analysis being conservative), probably owing to strain hardening and second order effects at very large deformation levels which are not accounted for in the analysis.

It is noteworthy that the experimental behaviour of beam B2-J presented in the plot of Fig. 2(a) attests clearly that flexural yielding occurred prior to shear failure. However, the failure mode of this specimen showed in Fig. 3(a) reveals that the beam finally exhibited shear diagonal failure. This is justified by the fact that the shear strength of the specimen B2-J is lower than its ultimate flexural capacity. The recorded post-yield hardening plateau corresponds to a mid-span displacement ductility in the range of 11 (see Table 2), which, although not as extensive as that seen in the other specimens of the B series, is yet significant. So there is no dispute over the occurrence of flexural yielding with sustained deformation capacity. Yet, in the end, after all this significant amount of ductile deflection, shear failure prevailed as shown in the figure of the final state (Fig. 3(a)), due to the relatively sparse spacing of stirrups.

4.3. The role of shear stress demand at the interface

To better illustrate the influence of the shear transfer at the interface, the composite cross section is disassembled to its two components, namely the encased existing rectangular cross section or the original beam and a U-shape shell section representing the jacket, respectively (Fig. 14). For any curvature magnitude, ϕ, acting on the composite cross-section, the two

components are analysed separately in flexure, keeping the same depth of compression zone, c, as that which was found developing in the composite cross section. Both components produce an axial stress resultant, N, of equal magnitude and opposite sign. The axial force is transferred from the internal core to the outer shell through the interface in the form of shear stress flow, τ. Hence, the shear stress demand at the interface may be determined from the axial stress resultant of the shell section when analysed in flexure, for the curvature value experienced by the composite cross section. Thus, at every loading step k, for the associated curvature ϕ_k and the corresponding height of the compression zone c_k, the shear stress demand was estimated:

$$\tau_{d,k} = \frac{N_k}{(C_{cr}/2)\cdot b_J + 2\cdot(C_{cr}/2)\cdot h_o} \tag{12}$$

where N_k is the force resultant at k step of the analysis of the jacket shell cross section, C_{cr} is the crack spacing (it is reminded that reversal of shear flow occurs at the mid-interval between adjacent cracks). Eq. (12) considers that the shear stress is uniformly distributed along the lateral interfaces due to the existence of dowels at the lateral interfaces. The variation of the estimated shear stress demand with curvature for beams A1-J and B1-J is depicted in Fig. 15. The shear stress demand - curvature curve could be divided in three distinct regions. The first region is characterized by an ascending branch up to a peak value. In this region, the force resultant increases implying that both the concrete and steel stresses increase. The second region is characterized by a descending branch where concrete stresses increase and steel stresses reach their yield strength in the plateau. In the last region, the curve has a positive slope denoting that the force resultant increases due to the simultaneous reduction of the concrete stresses (due to compression softening beyond the peak point) and the increase of steel stresses due to strain hardening. At this advanced stage of response, it is considered that the main shear stress capacity of the bottom and lateral interfaces is provided by the yielding dowel forces of the jacket stirrup legs and the L-shaped mild steel dowels, respectively. (This

is a conservative assumption, ignoring the contribution of friction to the total shear strength.) The estimated shear stress capacity of the bottom and lateral interfaces are depicted with the dashed horizontal lines in Fig. 14; values are estimated using Eq. (6). The shear capacity is higher than the shear demand in case of the bottom interface of beam A1-J and both bottom and lateral interfaces of beam B1-J, implying that the interface will remain intact, justifying the observed monolithic response. The shear stress capacity is lower than demand only in the lateral interfaces of beam A1-J, indicating that some slip (and subsequent interface failure) would be anticipated.

Thus, in the cases of monolithic response, it was shown that the response of the jacketed cross section is identical to the response resulting from the summation of the responses of the two components of the composite section, i.e. shell and core (Fig. 15). The moment curvature analysis of the shell is conducted for the same curvature, ϕ_k, and height of compression zone, c_k, as in the composite cross section. The force resultant, N_k, is applied as external load for force equilibrium at the core cross section when studied separately. This procedure was implemented in beams A1-J and B1-J and the moment –curvature response curves of the individual components appear in Fig. 16. The moment – curvature response curves of the shell and the core section are denoted as "Shell (N#0)" and "Old for N#0".Summing up the moments corresponding to these two components for each curvature value, results in the moment value of the monolithic response curve (Shell (#0) + Old for N#0=Monolithic).This procedure was followed for all the beams thereby confirming the observed monolithic behaviour wherever it occurred.

5. Conclusions

The experimental evidence illustrates that the thin reinforced concrete jackets combine a higher performance efficiency than conventional RC jackets with several of the advantages of

other retrofit solutions, such as those of synthetic composite jackets (ultra-thin layer, easily placeable), the reliability of steel, and the improved protection provided by mortar as compared with the resin matrices of conventional FRPs. Application of this technique to flexural members which had been heavily damaged during previous loading was shown to lead to full recovery and even to a remarkable increase of strength with enhanced ductility capacity and favourable failure modes. The analytical model developed in order to evaluate specimen response, accounting for the constitutive properties of the frictional interface, was used to interpret the mechanics of the composite jacketed element and to correlate the test results. Slip relieves stress concentration at the interface, contributing significantly to the deformation capacity of the member in a manner that differs from conventional flexural curvature. A practical result of the study was establishing documented evidence as to the efficacy of reinforced SCC jackets as a quick rehabilitation option for earthquake-damaged members, as an easily applicable retrofit scheme relying on familiar application techniques from conventional concrete and using readily available materials.

References

[1] Karayannis CG, Chalioris CE Sirkelis GM. Local retrofit of exterior RC beam-column joints using thin RC jackets - An experimental study. Earthquake Engineering and Structural Dynamics 2008;37(5):727-746.

[2] Thermou GE, Pantazopoulou SJ. Metallic fabric jackets: An innovative method for seismic retrofitting of substandard RC prismatic members. Structural Concrete 2007;8(1):35-46.

[3] Triantafillou TC, Papanicolaou CG. Shear strengthening of reinforced concrete members with textile reinforced mortar (TRM) jackets. Materials and Structures 2006;39(285):93-103.

[4] Si Larbi A, Contamine R, Ferrier E, Hamelin P. Shear strengthening of RC beams with textile reinforced concrete (TRC) plate. Construction and Building Materials 2010;24(10):1928-1936.

[5] Morshedt R, Kazemi MT. Seismic shear strengthening of R/C beams and columns with expanded steel meshes. Structural Engineering and Mechanics 2005;21(3):333-350.

[6] Manos GC, Katakalos K, Papakonstantinou CG. Shear behavior of rectangular beams strengthened with either carbon or steel fiber reinforced polymers. Applied Mechanics and Materials 2011;82:571-576.

[7] Al-Salloum YA, Elsanadedy HM, Alsayed SH, Iqbal RA. Experimental and numerical study for the shear strengthening of reinforced concrete beams using textile-reinforced mortar. J Composites for Construction 2012;16(1):74-90.

[8] Martinola G, Meda A, Plizzari GA, Rinaldi Z. Strengthening and repair of RC beams with fiber reinforced concrete, Cement and Concrete Composites 2010;32(9):731-739.

[9] Meda A, Plizzari, G.A., Rinaldi, Z., Martinola, G. Strengthening of R/C existing columns with high performance fiber reinforced concrete jacket. In: Proceedings of the 2nd International Conference on Concrete Repair, Rehabilitation and Retrofitting, ICCRRR, Concrete Repair, Rehabilitation and Retrofitting II 2009; p. 443-444.

[10] D'Ambrisi A, Focacci F. Flexural Strengthening of RC Beams with Cement-Based Composites. J Composites for Construction 2011;15(5):707-720.

[11] Gillum, A.J., Shahrooz, B.M., Cole, J.R. Bond strength between sealed bridge decks and concrete overlays. ACI Structural Journal 2001;98(6):872-879.

[12] Bousias SN, Biskinis D, Fardis MN, Spathis A-L. Strength, stiffness, and cyclic deformation capacity of concrete jacketed members. ACI Structural J 2007;104(5):521-531.

[13] Tsonos A-DG. Performance enhancement of R/C building columns and beam-column joints through shotcrete jacketing. Engineering Structures 2010;32(3):726-740.

[14] Chrysostomou CZ, Kyriakides N, Kotronis P, Poljanšek M, Taucer F, Roussis P, Kosmopoulos A. Seismic retrofitting of RC frames with RC infilling. In: Proceedings, 15th world Conference on earthquake engineering, Lisbon 2012; Paper 4144.

[15] Lampropoulos AP, Tsioulou OT, Dritsos SE. Monolithic coefficient values for design when seismically strengthening RC columns with jackets. Journal of Earthquake Engineering 2012;16(7):1023-1042.

[16] Lampropoulos AP, Dritsos SE. Modeling of RC columns strengthened with RC jackets, Earthquake Engineering and Structural Dynamics 2011;40(15):1689-1705.

[17] Tsonos AG. Effectiveness of CFRP-jackets and RC-jackets in post-earthquake and pre-earthquake retrofitting of beam-column subassemblages. Engineering Structures 2008;30(3):777-793.

[18] Karayannis CG, Sirkelis GM. Strengthening and rehabilitation of RC beam-column joints using carbon-FRP jacketing and epoxy resin injection. Earthquake Engineering and Structural Dynamics 2008;37(5):769-790.

[19] Thermou GE, Tastani SP, Pantazopoulou SJ. The effect of previous damage on the effectiveness of FRP-jacketing for seismic repairs of RC structural members. ACI Special Publication 2011;2(275 SP):951-969.

[20] Colalillo MA, Sheikh SA. Seismic retrofit of shear-critical reinforced concrete beams using CFRP. Construction and Building Materials 2012;32:99-109.

[21] Taljsten B Strengthening concrete beams for shear with CFRP sheets. Construction and Building Materials 2003;17:1-12.

[22] Deifalla A, Ghobarah A. Strengthening RC T-beams subjected to combined torsion and shear using FRP fabrics: Experimental study. J Composites for Construction 2010;14(3):301-311.

[23] Karayannis CG, Chalioris CE. Experimental investigation of the contribution of bonded C-FRP jackets to shear capacity of RC beams, Role of Cement Science in Sustainable Development - Proceedings of the International Symposium - Celebrating Concrete: People and Practice 2003; p. 689-696.

[24] Chen JF, Teng JG. Shear capacity of FRP-strengthened RC beams: FRP debonding. Construction and Building Materials 2003;17:24-41.

[25] Chaallal O, Shahawy M, Hassan M. Performance of reinforced concrete T-girders strengthened in shear with carbon fiber-reinforced polymer fabric. ACI Structural J 2002;99(3):335-343.

[26] Deniaud C, Cheng JJ. Shear behavior reinforced concrete T-beams with externally bonded fiber-reinforced polymer sheets. ACI Structural J 2001;98(3):386-394.

[27] Triantafillou TC. Shear strengthening of reinforced concrete beams using epoxy-bonded FRP composites," ACI Structural J 1998;95(2):107-115.

[28] Chalioris CE. Analytical model for the torsional behaviour of reinforced concrete beams retrofitted with FRP materials. Engineering Structures 2007;29(12):3263-3276.

[29] Tsonos AG. Effectiveness of CFRP-jackets in post-earthquake and pre-earthquake retrofitting of beam-column subassemblages. Structural Engineering and Mechanics 2007;27(4):393-408.

[30] Gil-Martín LM, Aschheim M, Hernández-Montes E, Pasadas-Fernández M. Recent developments in optimal reinforcement of RC beam and column sections. Engineering Structures 2011;33(4):1170-1180.

[31] Favvata, M.J., Izzuddin, B.A., Karayannis, C.G. Modelling exterior beam-column joints for seismic analysis of RC frame structures. Earthquake Engineering and Structural Dynamics 2008;37(13):1527-1548.

[32] Chalioris CE, Pourzitidis CN. Rehabilitation of shear-damaged reinforced concrete beams using self-compacting concrete jacketing. ISRN Civil Engineering 2012;816107:12.

[33] Chalioris CE, Papadopoulos CP, Pourzitidis CN, Fotis D, Sideris KK. Application of a reinforced self-compacting concrete jacket in damaged reinforced concrete beams under monotonic and repeated loading. J Engineering 2013;912983:12.

[34] Chalioris CE, Pourzitidis CN, Papadopoulos CP, Fotis D. Flexural rehabilitation of RC beams using self-compacting concrete jacketing. Advances in Civil Engineering and Building Materials: Proceedings 2nd International Conference on Civil Engineering and Building Materials (CEBM), Hong Kong 2012; p. 783-786.

[35] Tsioulou OT, Lampropoulos AP, Dritsos SE. Experimental investigation of interface behaviour of RC beams strengthened with concrete layers. Construction and Building Materials 2013;40:50-59.

[36] Achillopoulou VD, Karabinis IA. Investigation of shear transfer mechanisms in repaired damaged concrete columns strengthened with RC jackets. Structural Engineering and Mechanics 2013;47(4):575-598.

[37] Júlio ENBS, Branco FAB. Reinforced concrete jacketing - Interface influence on cyclic loading response, ACI Structural J 2008;105(4):471-477.

[38] Vandoros KG, Dritsos SE. Concrete jacket construction detail effectiveness when strengthening RC columns. Construction and Building Materials 2008;22(3):264-276.

[39] Tsonos AG. Lateral load response of strengthened reinforced concrete beam-to-column joints. ACI Structural J 1999;96(1):46-56.

[40] Thermou GE, Elnashai AS. Seismic retrofit schemes for RC structures and local-global consequences. Progress in Structural Engineering and Materials 2006;8(1):1-15.

[41] Thermou GE, Pantazopoulou SJ, Elnashai AS. Global interventions for seismic upgrading of substandard RC buildings. J Structural Engineering 2012;138(3):387-401.

[42] Thermou GE, Pantazopoulou SJ, Elnashai AS. Flexural behavior of brittle RC members rehabilitated with concrete jacketing. J Structural Engineering 2007;133(10):1373-1384.

[43] Greek Interventions Code. Earthquake Planning and Protection Organization, Athens; 2012.

[44] Vassilopoulou I, Tassios P. Shear transfer capacity along a RC crack under cyclic sliding. In: Proceedings fib Symposium, Technical Chamber of Greece, Athens, Greece 2003;Paper No. 271.

[45] Tassios TS, Vintzēleou E. Concrete-to-concrete friction. J Structural Engineering 1987;113(4):832-849.

[46] CEB-FIP Model Code 2010. First complete draft - volume 2. Bulletin 56. In: Comité Euro-International du Béton. Secretariat permanent. Case Postale 88, CH-1015 Lausanne, Switzerland; 2010.

[47] Vintzēleou E, Tassios TS. Mathematical models for dowel action under monotonic and cyclic conditions. Magazine of Concrete Research 1986;38(134):13-22.

[48] Vintzēleou E, Tassios TS. Behavior of dowels under cyclic deformations. ACI Structural J 1987;84(1):18-30.

[49] Eurocode 2. Design of concrete structures – Part 1-1: General rules and rules for buildings. EN 1992-1-1:2004. In: Comité Européen de Normalisation. Avenue Marnix 17, B-1000 Brussels, Belgium; 2004.

[50] Bentz EC, Collins MP. Response - 2000. Reinforced concrete sectional analysis using the modified compressiod field theory, Toronto; 2000.

[51] Vecchio FJ, Collins MP. The modified compression field theory for reinforced concrete elements subjected to shear. J ACI 1986;83(2):219-231.

LIST OF TABLES

LIST OF FIGURES

Table

Table 1. Geometrical, mechanical and steel reinforcement characteristics of the tested beams.

Initial beam name	Characteristics of the initial beams						$f_{c,o}$ / $f_{ct,o}$ (MPa)	Jacketed beam name	Characteristics of the jackets** and the jacketed beams							$f_{c,J}$ / $f_{ct,J}$ (MPa)	Total reinforcement	
	b_o/h_o (mm)	d_o (mm)	a/d_o	Longitudinal bars top	Longitudinal bars bottom	Stirrups			b_J/h_J (mm)	d_J (mm)	a/d_J	Longitudinal bars top	Longitudinal bars middle	Longitudinal bars bottom	U-formed stirrups		ρ_l	ρ_t
A1	200/300	275	2.91	2∅14 *(0.56%)*	2∅14 *(0.56%)*	∅8/200 *(0.25%)*	27.6 / 2.20	A1-J	250/325	305	2.62	2∅5 *(0.05%)*	2∅5 *(0.05%)*	16∅5 *(0.41%)*	∅5/50 *(0.31%)*	43.8 / 3.41	*0.82%*	*0.52%*
A2	200/300	275	2.18	3∅16 *(1.10%)*	3∅16 *(1.10%)*	None *(0.00%)*	26.2 / 2.10	A2-J	250/325	305	1.97	2∅5 *(0.05%)*	2∅5 *(0.05%)*	6∅5 *(0.15%)*	∅5/25 *(0.63%)*	43.9 / 3.54	*0.95%*	*0.63%*
B1	125/200	175	3.43	4∅8 *(0.92%)*	2∅8 *(0.46%)*	∅5/150 *(0.21%)*	25.5 / 2.07	B1-J	175/225	205	2.93	2∅5 *(0.11%)*	2∅5 *(0.11%)*	4∅5 *(0.22%)*	∅5/200 *(0.11%)*	43.0 / 3.62	*0.50%*	*0.26%*
B2	125/200	175	3.43	4∅8 *(0.92%)*	2∅8 *(0.46%)*	∅5/300 *(0.10%)*	28.2 / 2.15	B2-J	175/225	205	2.93	2∅5 *(0.11%)*	2∅5 *(0.11%)*	4∅5 *(0.22%)*	∅5/150 *(0.15%)*	42.8 / 3.72	*0.50%*	*0.22%*
B3	125/200	175	3.43	2∅8 *(0.46%)*	4∅8 *(0.92%)*	∅5/300 *(0.10%)*	27.2 / 2.20	B3-J	175/225	205	2.93	2∅5 *(0.11%)*	2∅5 *(0.11%)*	2∅5 *(0.11%)*	∅5/80 *(0.28%)*	40.5 / 3.47	*0.67%*	*0.36%*
B3R*	125/200	175	3.43	2∅8 *(0.46%)*	4∅8 *(0.92%)*	∅5/300 *(0.10%)*	27.1 / 2.11	B3R-J*	175/225	205	2.93	2∅5 *(0.11%)*	2∅5 *(0.11%)*	2∅5 *(0.11%)*	∅5/80 *(0.28%)*	40.2 / 3.42	*0.67%*	*0.36%*
B4	125/200	175	3.43	4∅8 *(0.92%)*	4∅8 *(0.92%)*	∅5/200 *(0.16%)*	23.4 / 2.05	B4-J	175/225	205	2.93	2∅5 *(0.11%)*	2∅5 *(0.11%)*	2∅5 *(0.11%)*	∅5/100 *(0.22%)*	40.0 / 3.25	*0.67%*	*0.34%*
B4R*	125/200	175	3.43	4∅8 *(0.92%)*	4∅8 *(0.92%)*	∅5/200 *(0.16%)*	25.7 / 2.06	B4R-J*	175/225	205	2.93	2∅5 *(0.11%)*	2∅5 *(0.11%)*	2∅5 *(0.11%)*	∅5/100 *(0.22%)*	40.1 / 3.34	*0.67%*	*0.34%*
B5	125/200	175	3.43	2∅8 *(0.46%)*	4∅8 *(0.92%)*	∅5/150 *(0.21%)*	23.8 / 1.95	B5-J	175/225	205	2.93	2∅5 *(0.11%)*	2∅5 *(0.11%)*	2∅5 *(0.11%)*	∅5/100 *(0.22%)*	39.8 / 3.32	*0.67%*	*0.37%*
B5R*	125/200	175	3.43	2∅8 *(0.46%)*	4∅8 *(0.92%)*	∅5/150 *(0.21%)*	26.2 / 2.07	B5R-J*	175/225	205	2.93	2∅5 *(0.11%)*	2∅5 *(0.11%)*	2∅5 *(0.11%)*	∅5/100 *(0.22%)*	40.0 / 3.31	*0.67%*	*0.37%*

* Beams tested under repeated loading (all the other specimens tested under monotonic loading)

** Mix design proportions of SCC of the jackets (kg/m^3): CEM II M/42.5N: 305, CEM IV (W-P)B 32.5N: 51, Limestone filler: 101, Limestone sand: 882, Coarse aggregates (4/8 mm): 800, Water: 193, Superplasticizer: 11.93, Retarder: 1.14, VMA: 0.43.

Table 2. Experimental results.

Beam name	P_{flex} (kN)	P_{diag} (kN)	P_y (kN)	Δ_{Py} (mm)	P_u (kN)	Δ_{Pu} (mm)	Δ_{max}/Δ_{Py}	Failure mode
A1	29.6	58.7	109.9	7.46	130.5	93.65	16.1	Flexure
A1-J	44.7	93.4	210.8	9.34	231.9	25.03	**3.6**	Flexure
A2	43.7	77.8	$= P_u$	$= \Delta_{Pu}$	108.0	1.87	1.0	Shear
A2-J	47.2	112.4	315.3	4.79	322.3	6.21	**1.3**	Shear
B1	13.4	26.3	30.6	4.50	43.5	59.05	13.7	Flexure
B1-J	18.2	30.9	43.0	4.74	60.7	43.76	**10.8**	Flexure
B2	13.7	25.8	29.9	3.41	36.4	16.06	5.0	Flexure - Shear
B2-J	22.3	32.3	41.5	4.22	55.2	38.85	**11.0**	Flexure - Shear
B3	12.1	31.9	$= P_u$	$= \Delta_{Pu}$	56.2	5.49	1.0	Shear
B3-J	23.3	35.6	69.8	4.35	84.0	59.84	**23.2**	Flexure
B3R	13.6	27.1	$= P_u$	$= \Delta_{Pu}$	55.8	5.34	1.0	Shear
B3R-J	19.7	34.4	68.4	5.07	83.2	89.87	**22.9**	Flexure
B4	13.7	32.0	$= P_u$	$= \Delta_{Pu}$	57.2	5.62	1.0	Shear
B4-J	19.2	35.4	69.3	4.82	79.9	76.19	**21.7**	Flexure
B4R	13.1	31.6	$= P_u$	$= \Delta_{Pu}$	57.0	5.58	1.0	Shear
B4R-J	22.3	32.4	65.4	4.99	81.0	69.24	**21.6**	Flexure
B5	13.7	28.3	58.7	6.40	61.7	8.24	1.3	Shear
B5-J	23.3	32.9	70.8	5.34	83.0	59.25	**19.4**	Flexure
B5R	13.1	29.6	$= P_u$	$= \Delta_{Pu}$	58.2	5.88	1.0	Shear
B5R-J	19.7	31.9	69.8	5.58	79.4	84.15	**18.0**	Flexure

Figure

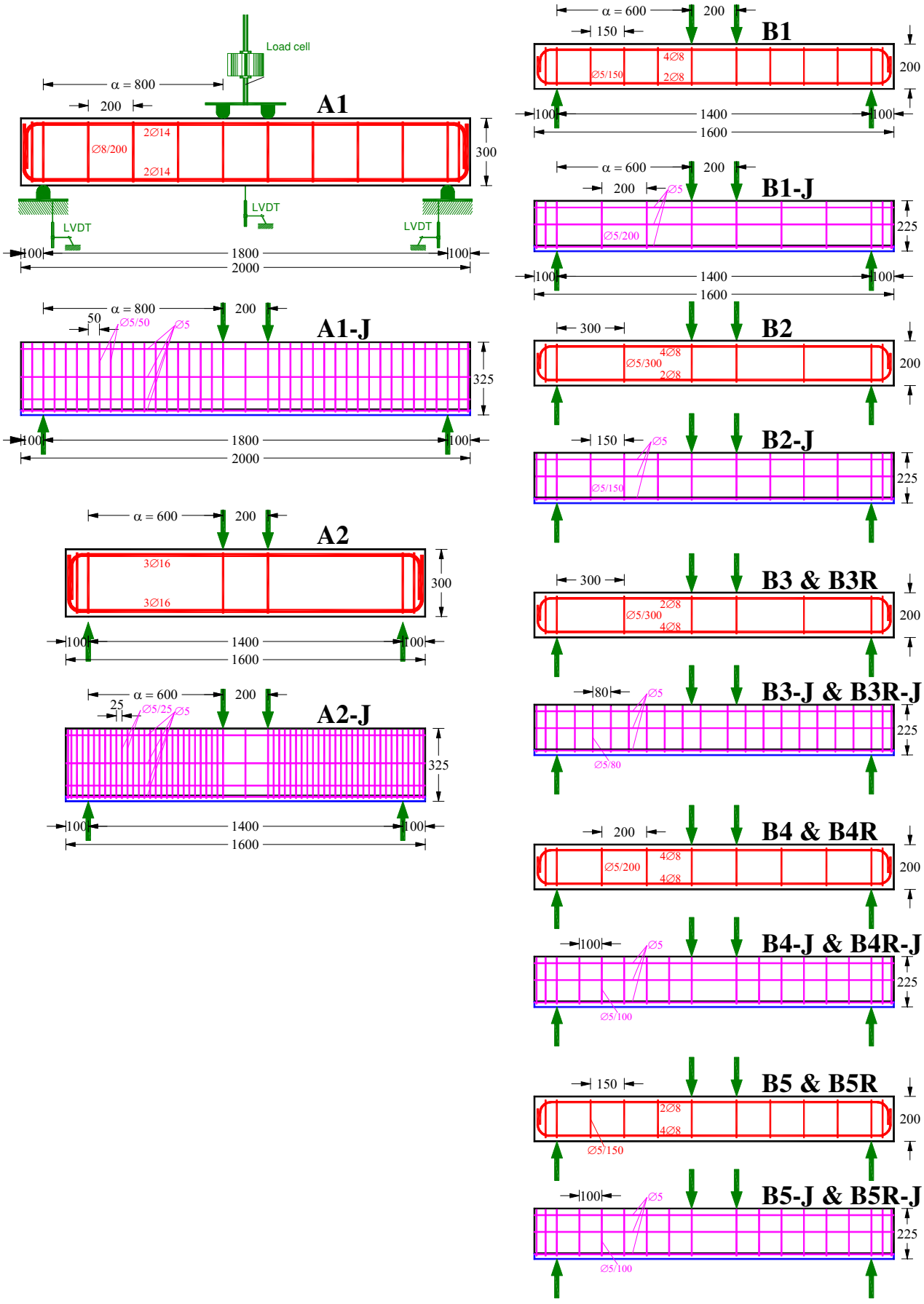

Figure 1. (a) Geometry, test setup and steel reinforcement arrangement of the tested beams.

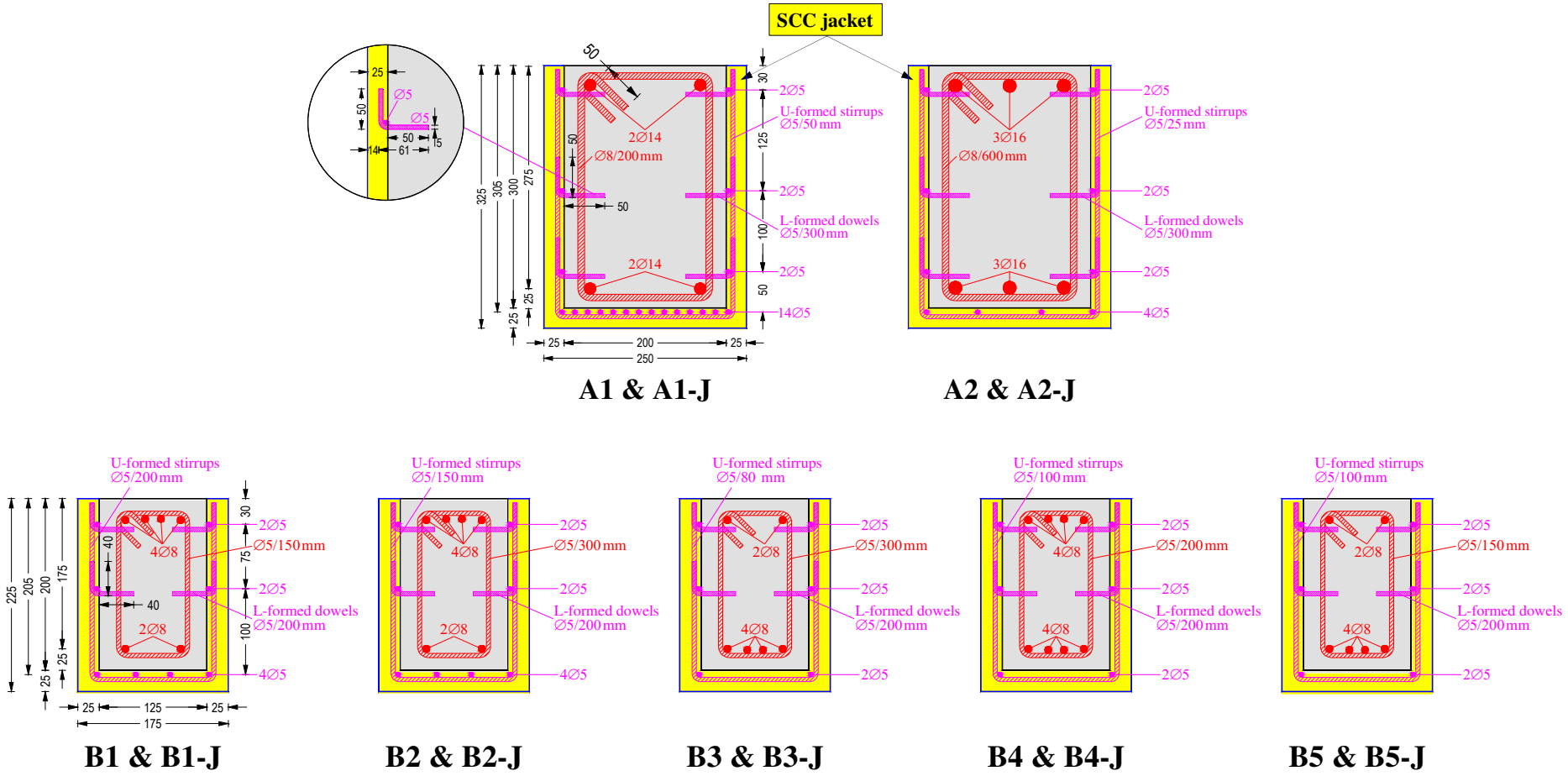

Figure 1. (b) Cross-sectional and steel reinforcement details of the tested beams.

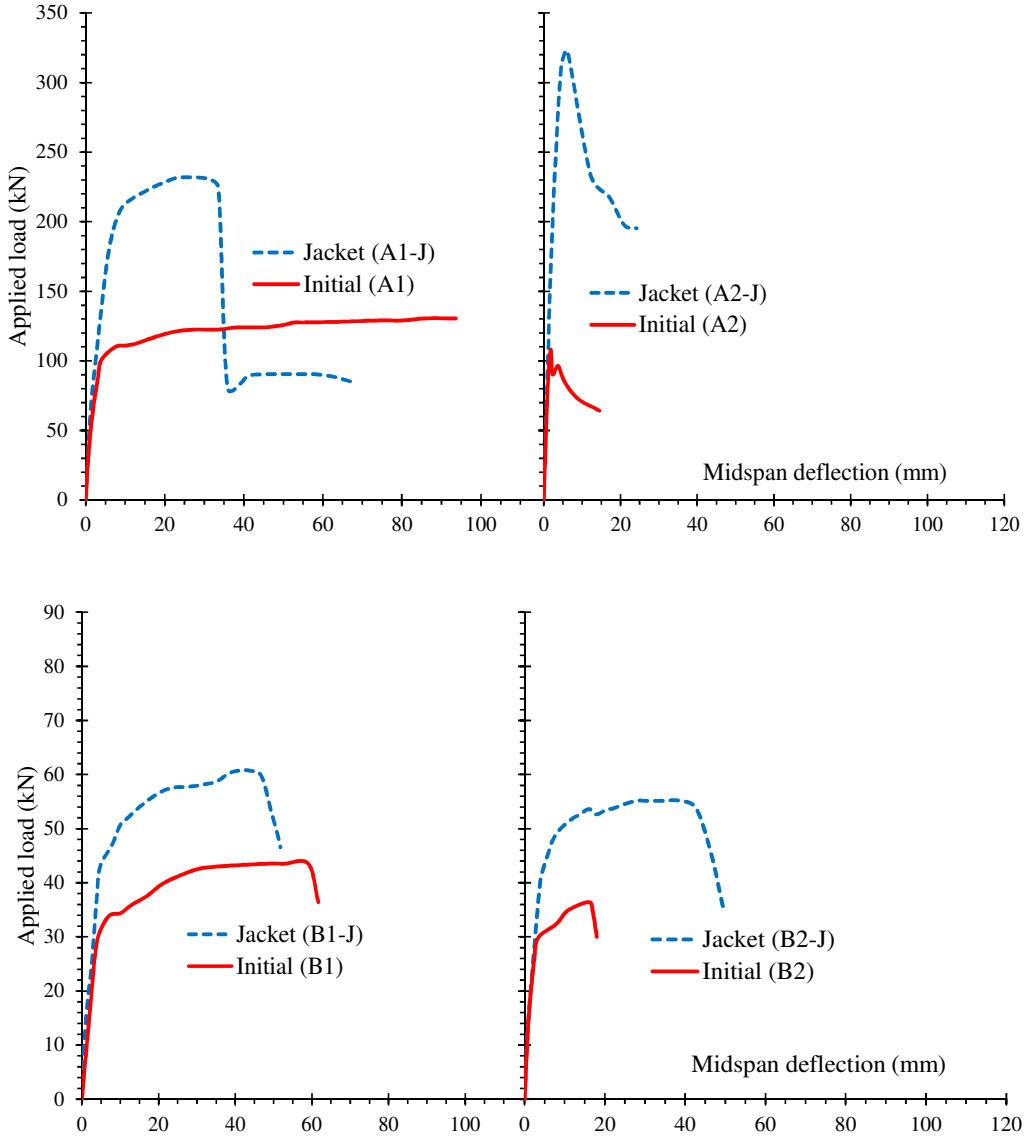

Figure 2a. Experimental behaviour of the tested beams.

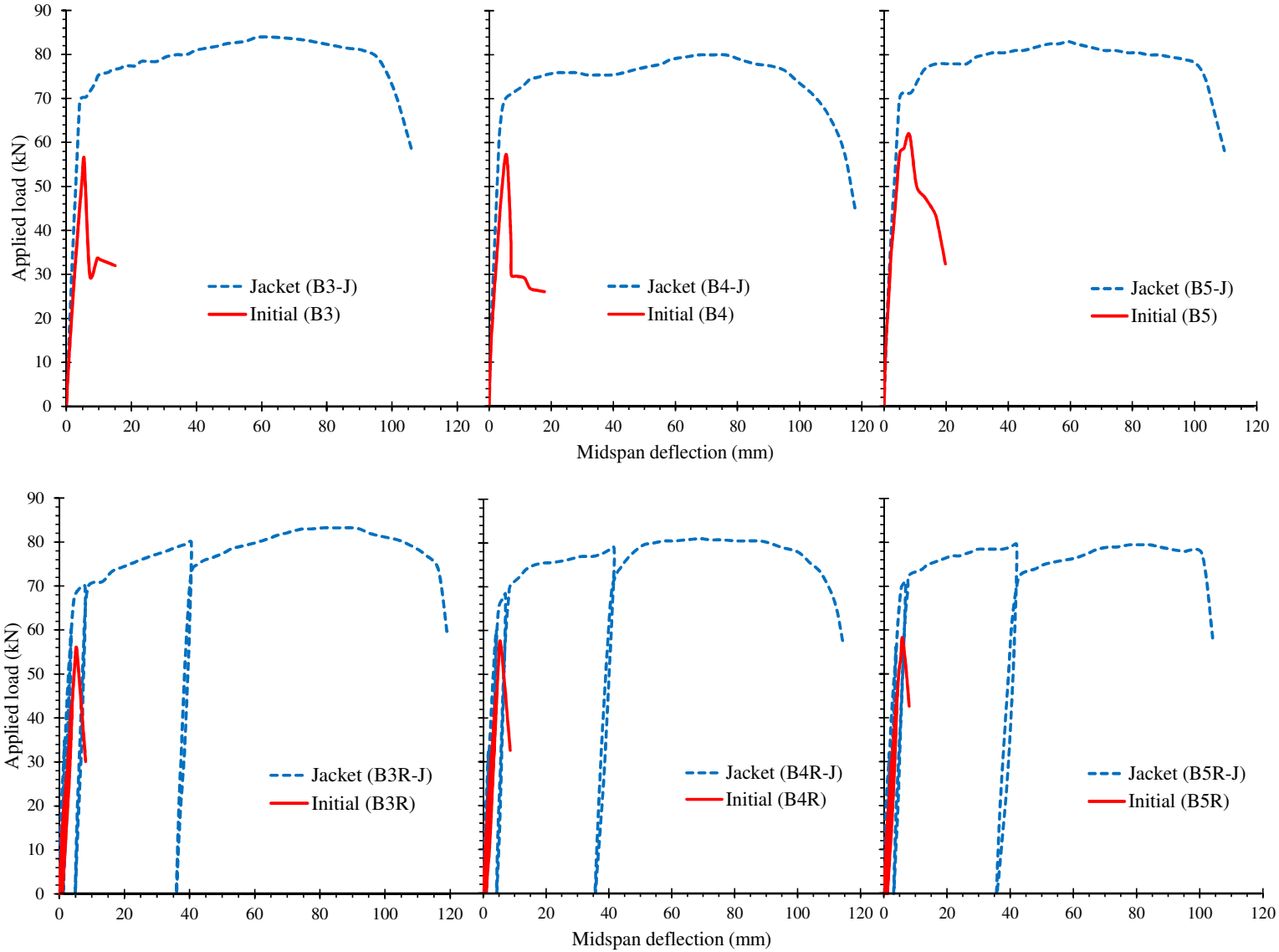

Figure 2b. Experimental behaviour of the tested beams.

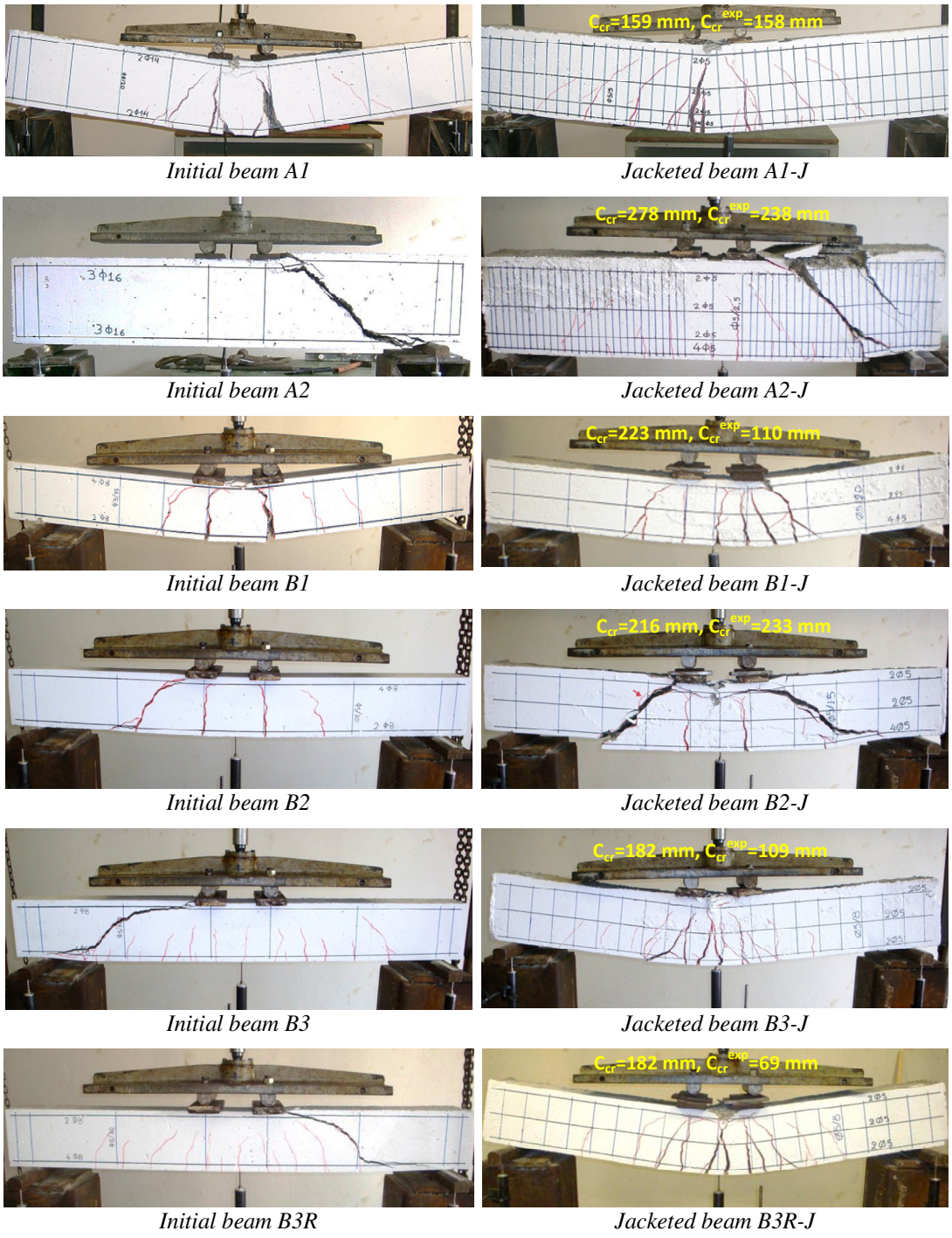

Initial beam A1 *Jacketed beam A1-J*

Initial beam A2 *Jacketed beam A2-J*

Initial beam B1 *Jacketed beam B1-J*

Initial beam B2 *Jacketed beam B2-J*

Initial beam B3 *Jacketed beam B3-J*

Initial beam B3R *Jacketed beam B3R-J*

Figure 3a. Cracking patterns of the original and the jacketed beams.

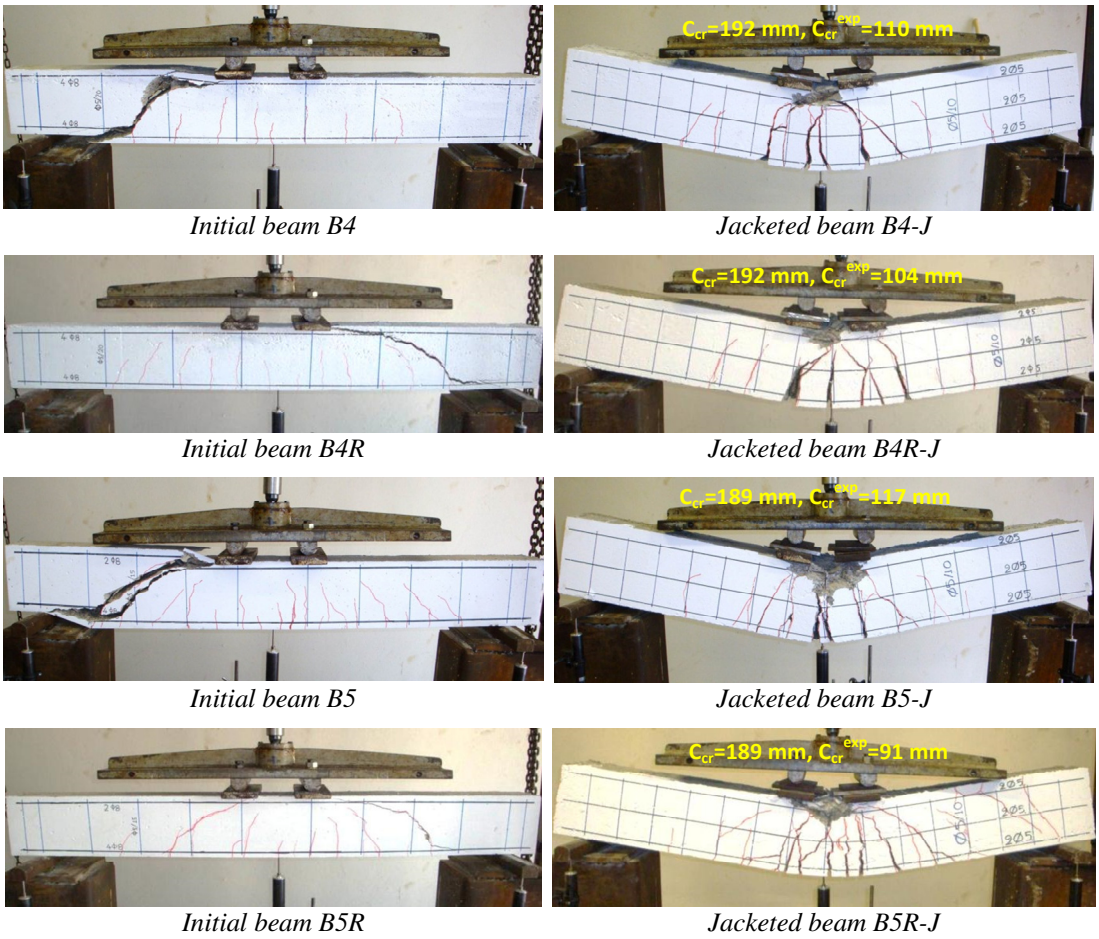

Initial beam B4 *Jacketed beam B4-J*

Initial beam B4R *Jacketed beam B4R-J*

Initial beam B5 *Jacketed beam B5-J*

Initial beam B5R *Jacketed beam B5R-J*

Figure 3b. Cracking patterns of the original and the jacketed beams.

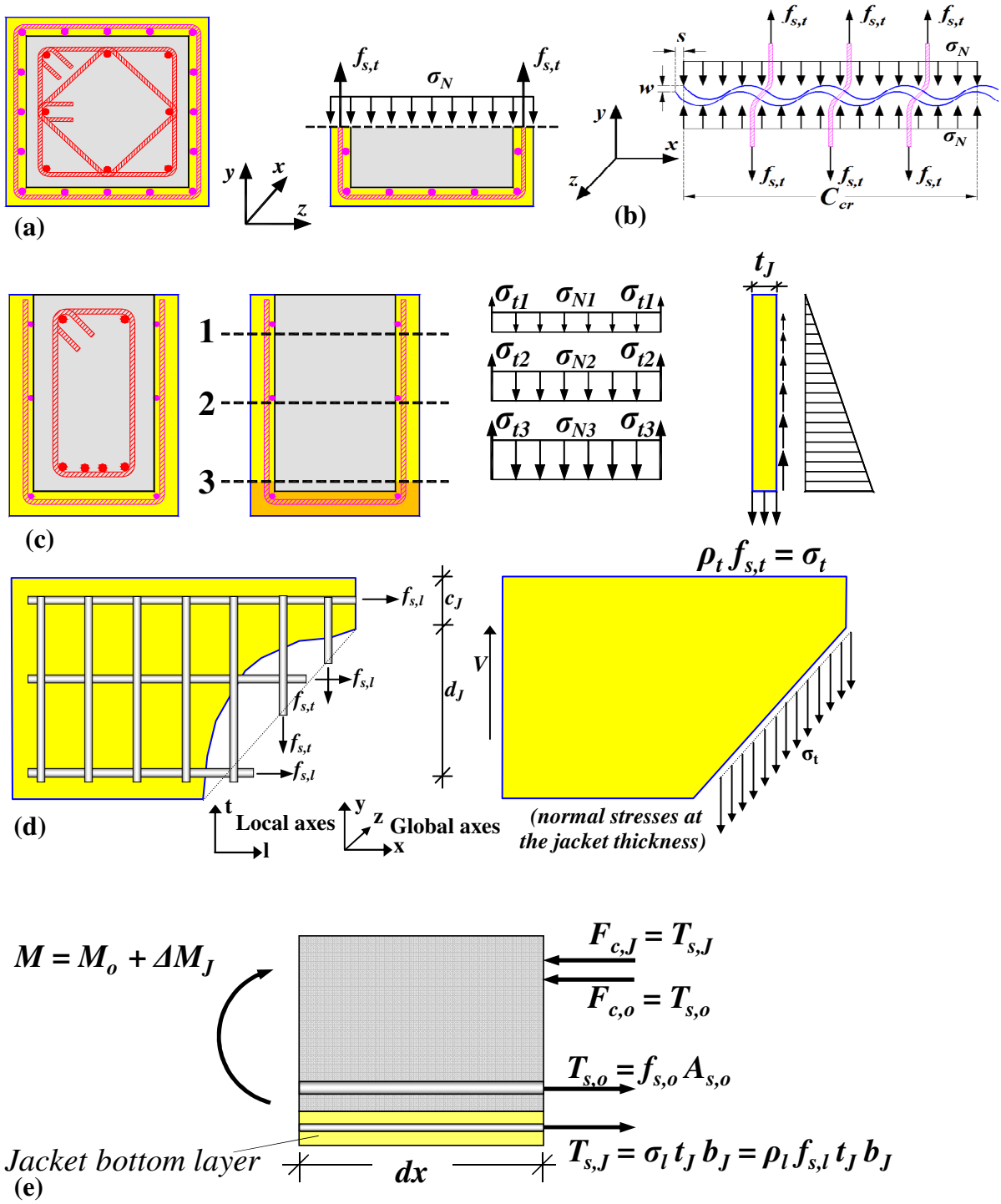

Figure 4. (a) Mobilization of confinement of the outer shell in four-sided jacket cross section. (b) Generation of passive confining action due to overriding of asperities. (c) Reduced effectiveness in three-sided jacket due to reduced restraint. (d) Contribution of the jacket to shear strength of the member. (e) Internal forces generated in the jacketed beam cross-section under flexural action.

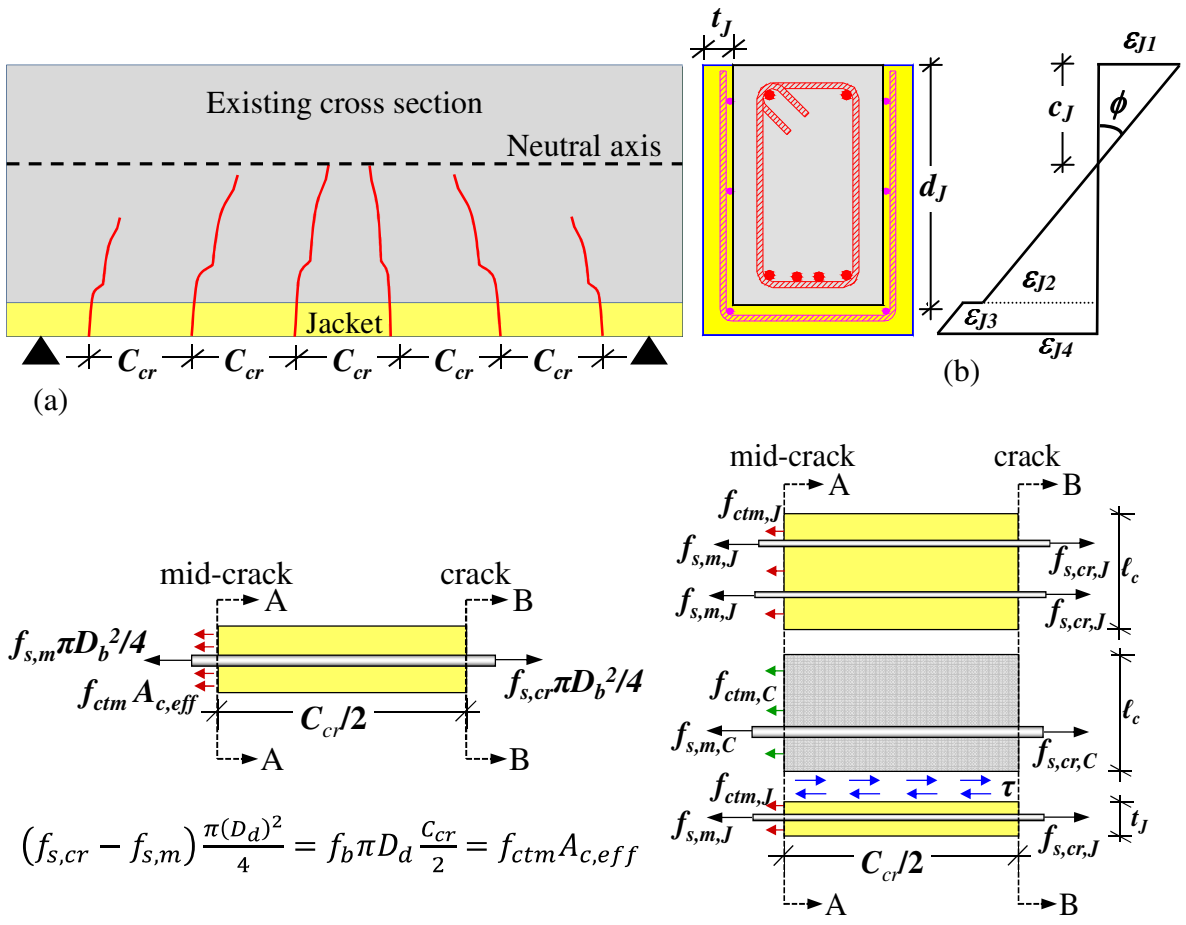

Figure 5. (a) Definition of crack spacing, C_{cr}, at crack stabilization. (b) Strain profile of the jacketed cross section. (c) Bar stresses at mid-distance between cracks (section A-A) and at crack (section B-B). (d) Free body equilibrium in the tension zone of the core of the composite section at sections A-A and B-B.

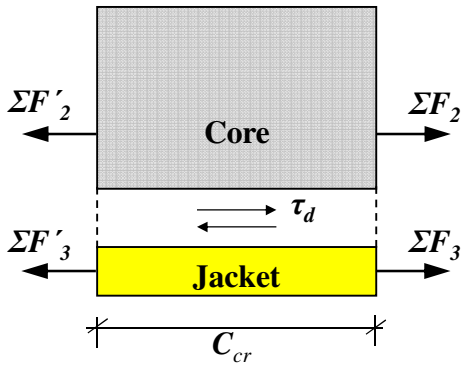

Figure 6. Section equilibrium between adjacent cracks.

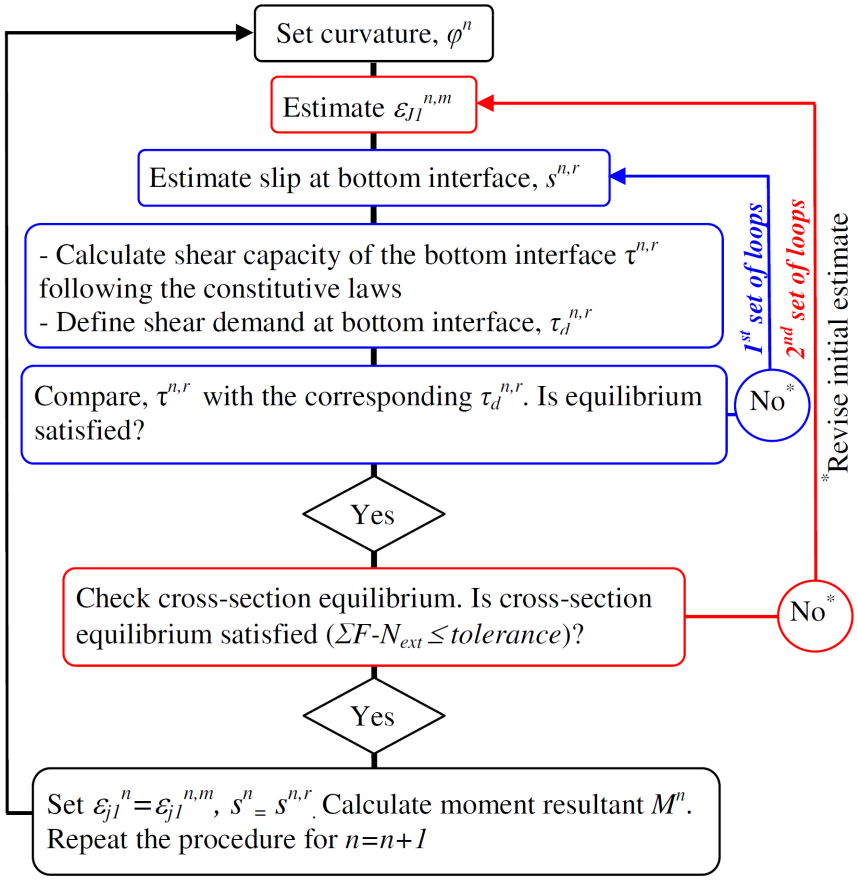

Figure 7. Flowchart of the proposed algorithm.

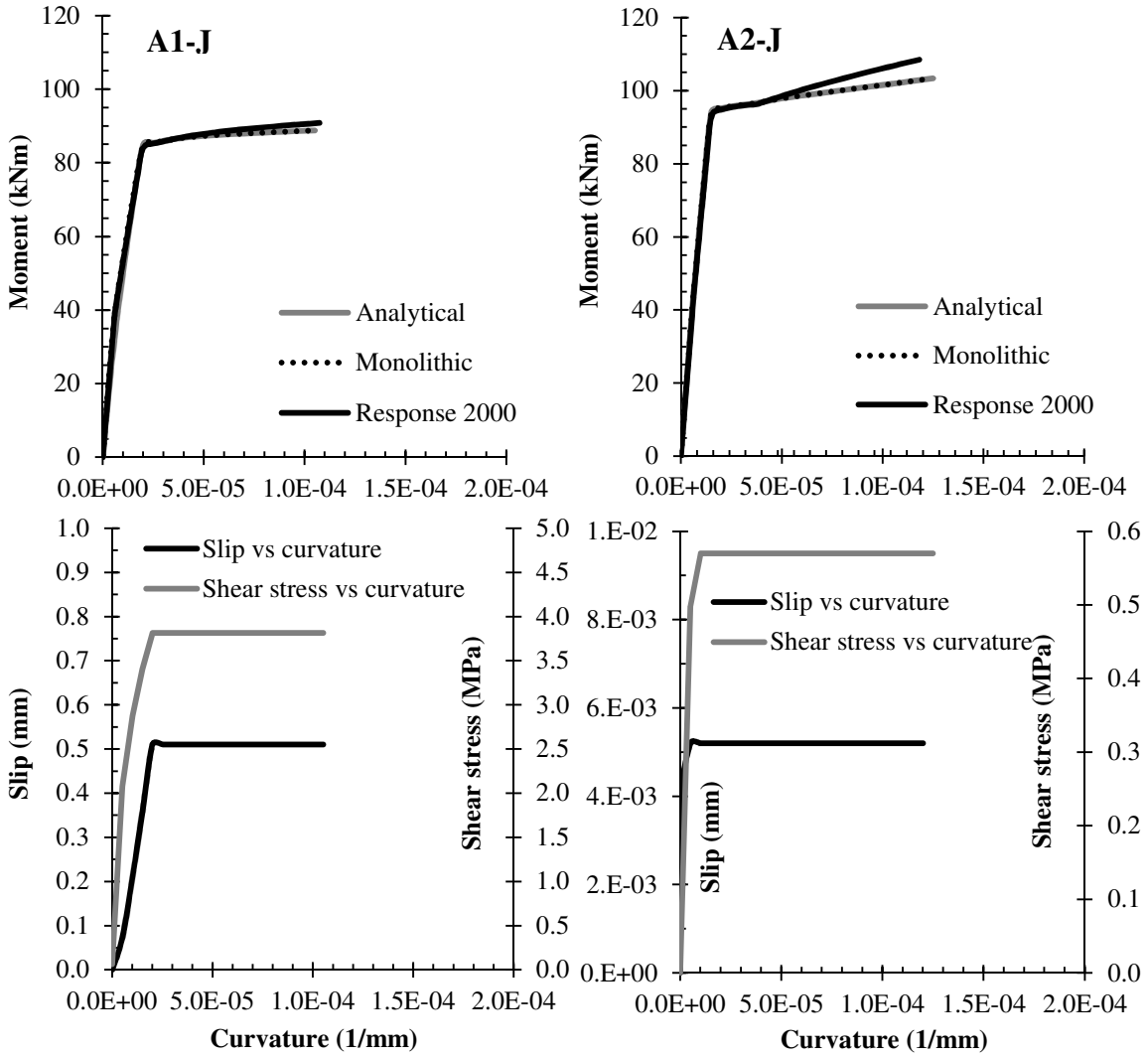

Figure 8. Moment versus curvature response curves and slip versus curvature - shear stress versus curvature relationship of beams of group A.

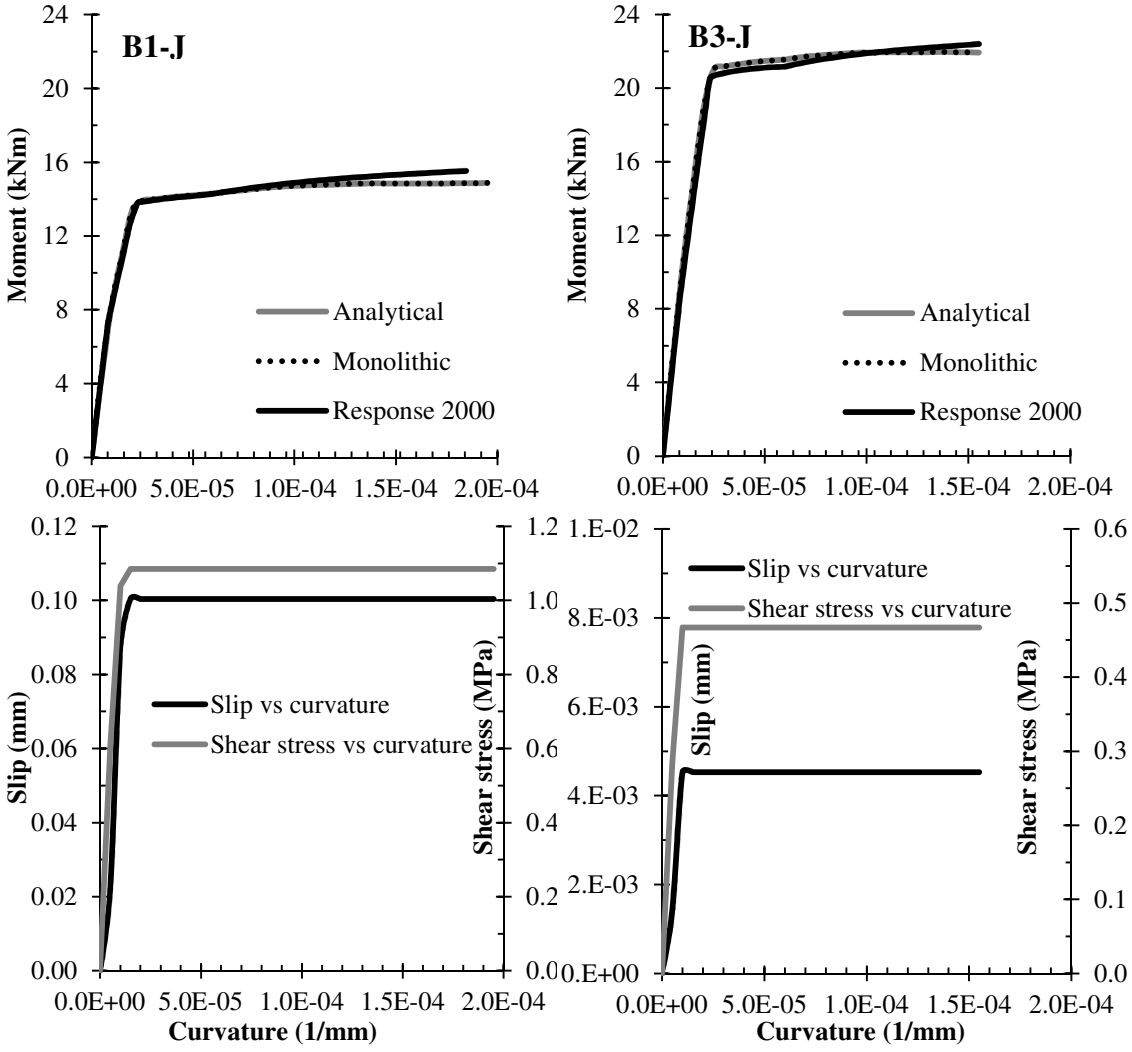

Figure 9. Moment versus curvature response curves and slip versus curvature - shear stress versus curvature relationship of beams of group B.

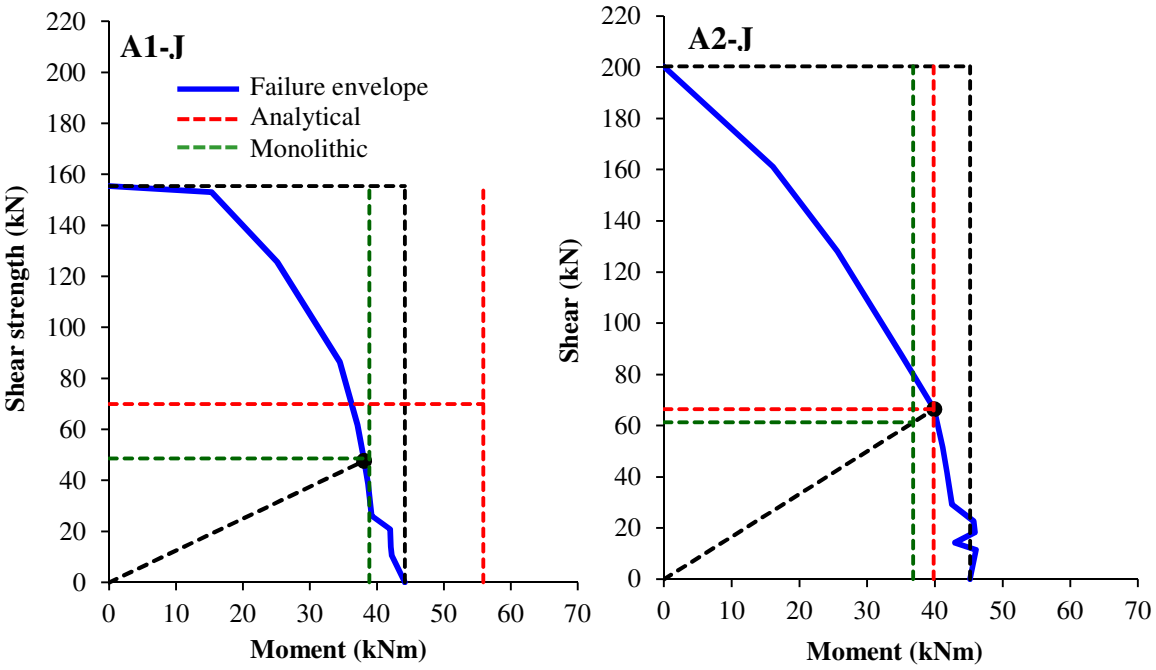

Figure 10. M-V interaction failure envelope at yielding of the bottom layer reinforcement of the jacketed beams of group A.

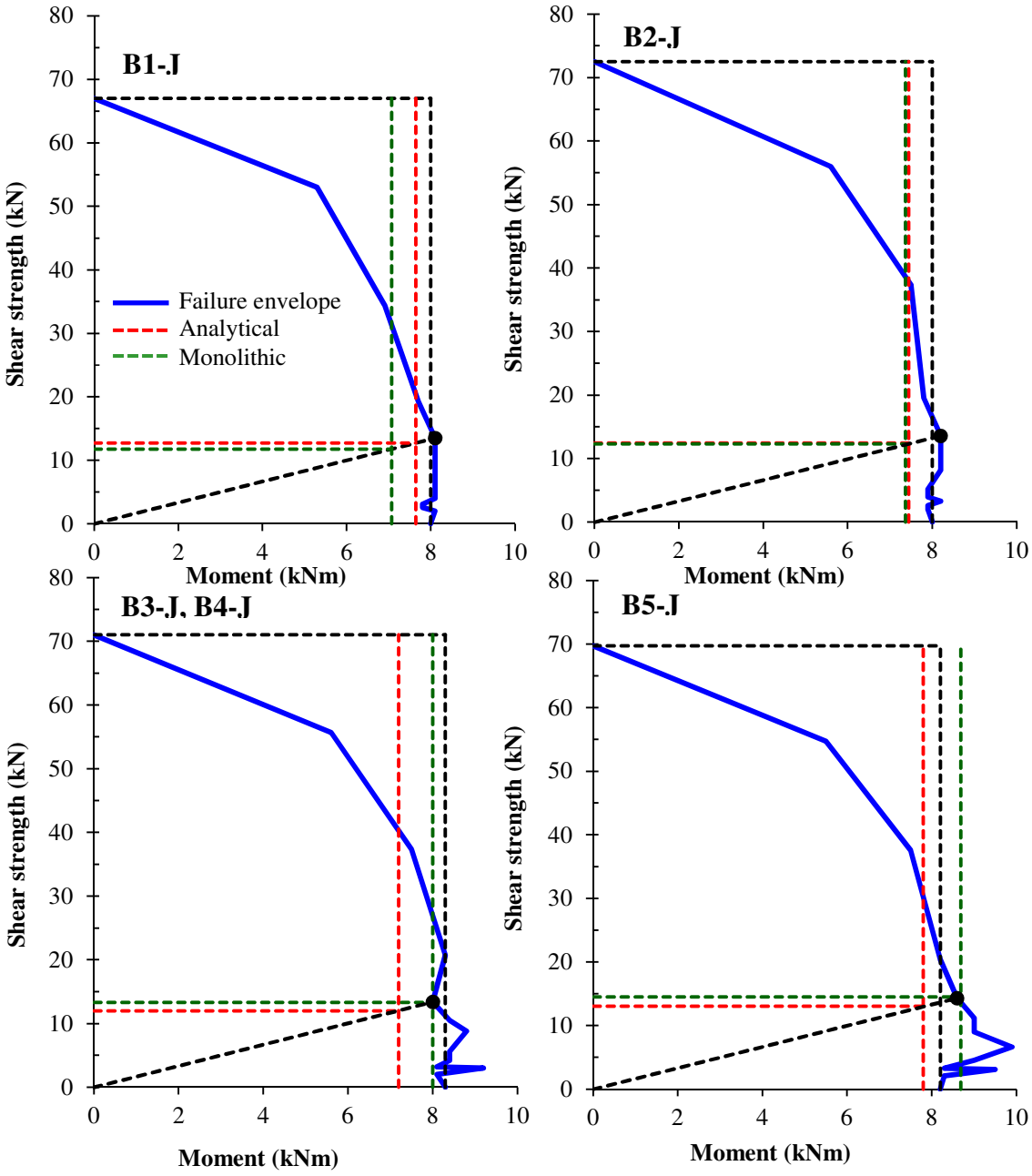

Figure 11. M-V interaction failure envelope at yielding of the bottom layer reinforcement of the jacketed beams of group B.

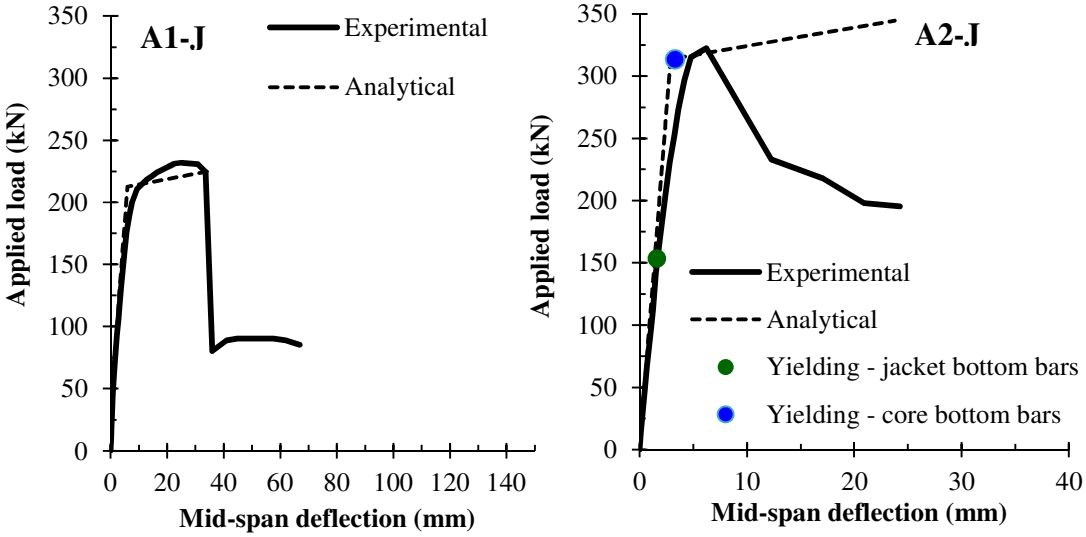

Figure 12. Applied load versus mid-span deflection curves of beams of group A.

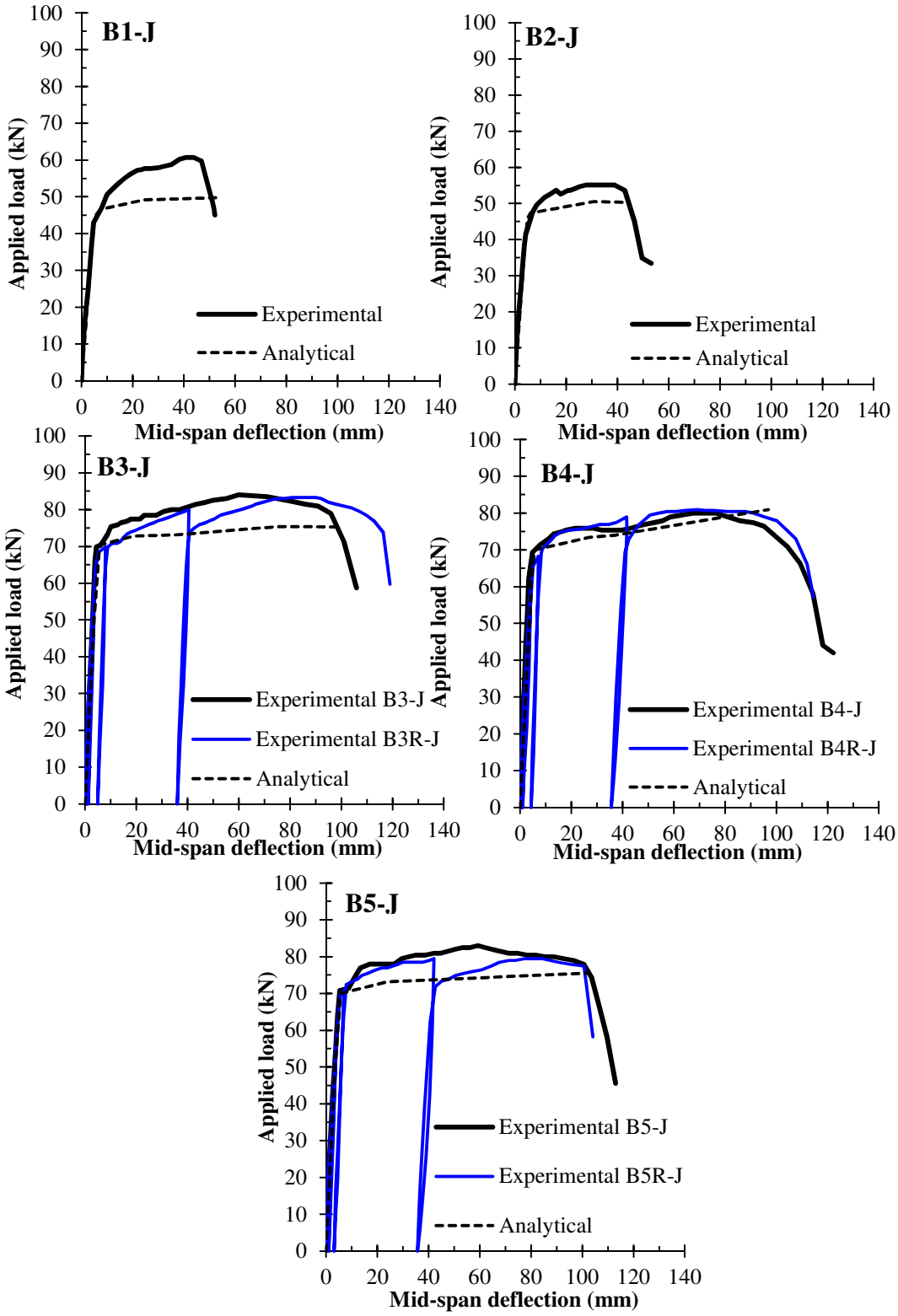

Figure 13. Applied load versus mid-span deflection curves of beams of group B.

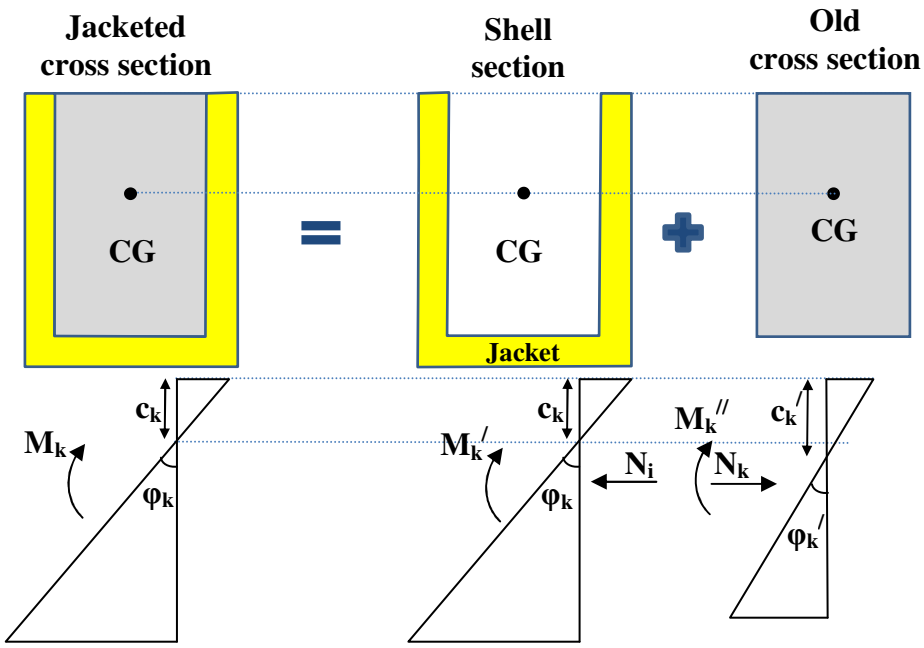

Figure 14. Decomposition of the composite cross section into shell and core section. Moment versus curvature analysis assumptions of the individual components for the case of monolithic response.

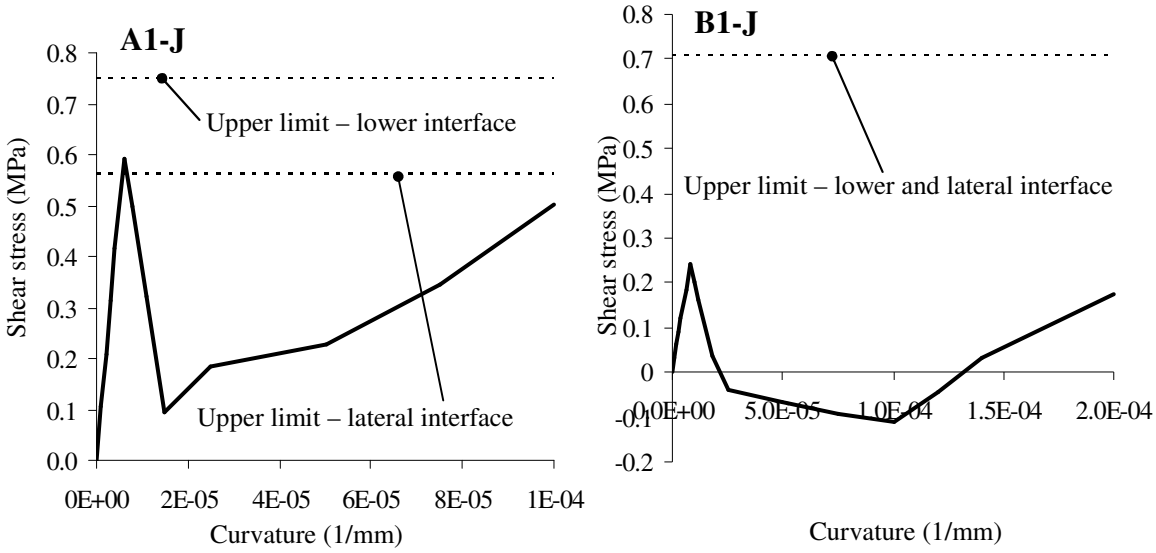

Figure 15. Shear stress capacity at the interface of the jacketed beams A1-J and B1-J.

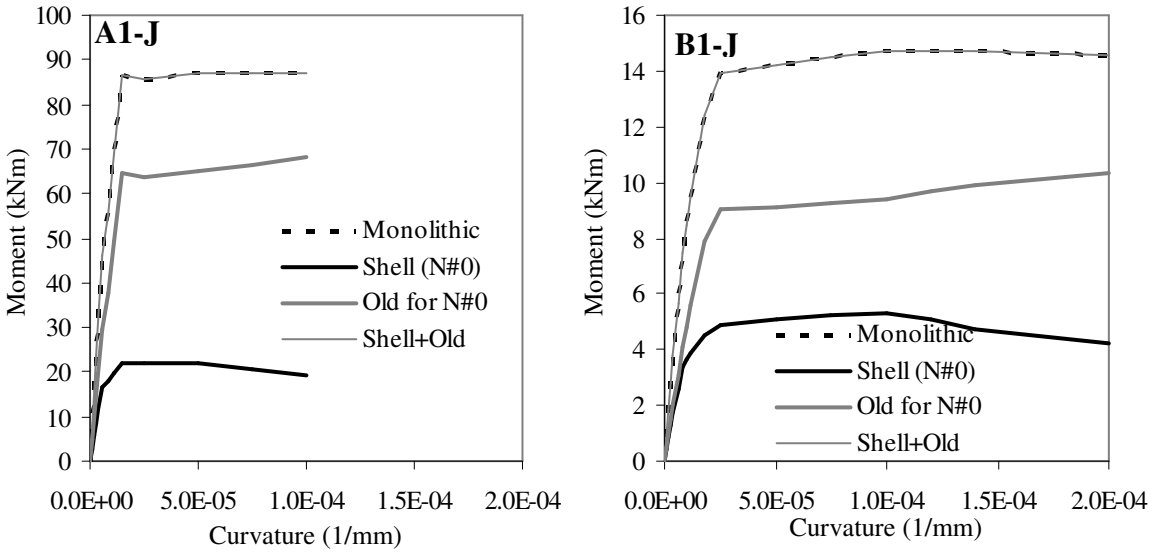

Figure 16. Moment versus curvature response of the composite cross section and individual component (shell and core).